Mon. Not. R. Astron. Soc. **336,** 449–466 (2002)

The origin of subdwarf B stars – I. The formation channels

Z. Han,[1⋆] Ph. Podsiadlowski,[2] P. F. L. Maxted,[3] T. R. Marsh[4] and N. Ivanova[2,5]

[1] *Yunnan Observatory, National Astronomical Observatories, Chinese Academy of Sciences, PO Box 110, Kunming, 650011, China*
[2] *Department of Astrophysics, University of Oxford, Oxford OX1 3RH*
[3] *Department of Physics, Keele University, Staffordshire ST5 5BG*
[4] *University of Southampton, Department of Physics and Astronomy, Highfield, Southampton SO17 1BJ*
[5] *Department of Physics and Astronomy, Northwestern University, Evanston, IL 60208, USA*

Accepted 2002 June 6. Received 2002 June 6; in original form 2002 February 27

ABSTRACT

Subdwarf B (sdB) stars (and related sdO/sdOB stars) are believed to be helium-core-burning objects with very thin hydrogen-rich envelopes. In recent years it has become increasingly clear from observational surveys that a large fraction of these objects are members of binary systems. To understand their formation better, we present the results of a detailed investigation of the three main binary evolution channels that can lead to the formation of sdB stars: the common-envelope (CE) ejection channel, the stable Roche lobe overflow (RLOF) channel, and the double helium white dwarfs (WDs) merger channel. The CE ejection channel leads to the formation of sdB stars in short-period binaries with typical orbital periods between 0.1 and 10 d, very thin hydrogen-rich envelopes and a mass distribution sharply peaked around $\sim$0.46 $M_\odot$. On the other hand, under the assumption that all mass transferred is soon lost, the stable RLOF channel produces sdB stars with similar masses but long orbital periods (400–1500 d) and with rather thick hydrogen-rich envelopes. The merger channel gives rise to single sdB stars whose hydrogen-rich envelopes are extremely thin but which have a fairly wide distribution of masses (0.4–0.65 $M_\odot$). We obtained the conditions for the formation of sdB stars from each of these channels using detailed stellar and binary evolution calculations where we modelled the detailed evolution of sdB stars and carried out simplified binary population synthesis simulations. The observed period distribution of sdB stars in compact binaries strongly constrains the CE ejection parameters. The best fits to the observations are obtained for very efficient CE ejection where the envelope ionization energy is included, consistent with previous results. We also present the distribution of sdB stars in the $T_{\rm eff}$–log g diagram, the Hertzsprung–Russell diagram and the distribution of mass functions.

Key words: methods: numerical – binaries: close – stars: formation – subdwarfs – white dwarfs.

1 INTRODUCTION

Subdwarf B (sdB) stars were originally defined by Sargent & Searle (1968) as stars with colours corresponding to those of B stars in which the Balmer lines are abnormally broad compared to those seen in Population I main-sequence stars. Subdwarf O (sdO) stars and subdwarf OB (sdOB) stars are related stars of correspondingly earlier spectral type (see e.g. Vauclair & Liebert 1987). Based on an interpretation of their evolutionary state, sdB stars are also sometimes referred to as extreme horizontal branch stars. They are generally considered to be helium-core-burning stars with extremely thin hydrogen envelopes (<0.02 $M_\odot$), and most of them are believed to have masses around 0.5 $M_\odot$ (Heber 1986; Saffer et al. 1994). Indeed, a recent asteroseismological analysis by Brassard et al. (2001) has confirmed a mass of $0.49 \pm 0.02\,M_\odot$ for the sdB star PG 0014 + 067. In this paper, we collectively refer to helium-core-burning stars with thin hydrogen envelopes as sdB stars if they are located in the corresponding region in a ($T_{\rm eff}$, log g) diagram, even if some of them may in reality be sdO or sdOB stars.

Subdwarf B stars form an important class of objects in several respects. At the Galactic level, they are the dominant population in surveys of blue objects (Green, Schmidt & Liebert 1986) and constitute a population of stars that are important for our understanding of the structure and evolution of the Galaxy. Pulsating sdB stars (Kilkenny et al. 1999) provide a standard candle for distance determinations. On a larger cosmological scale they have been used to constrain the ages of the oldest galaxies and hence

⋆E-mail: zhanwen@public.km.yn.cn

cosmological models. The latter is based on measuring the age of giant elliptical galaxies from the ultraviolet (UV) excess, or 'upturn', with the help of evolutionary population synthesis models where low-mass helium-core-burning stars provide the dominant source of UV radiation (Brown et al. 1997; Yi, Demarque & Oemler 1997; Yi et al. 1999).

More importantly, sdB stars are exotic objects because of their thin hydrogen-rich envelopes. Understanding the process of their formation helps to improve our understanding of the theory of stellar and binary evolution.

There have been extensive surveys of sdB stars in the past. Magnitude-limited and colour-selected samples have been obtained from the Palomar Green (PG) survey (Green et al. 1986) (magnitude limit $B \sim 16.1$) and the Kitt Peak Downes (KPD) survey (Downes 1986) (magnitude limit $B = 15.3$). Saffer et al. (1994) measured atmospheric parameters, such as effective temperature, surface gravity and photospheric helium abundance, for 68 sdB stars. Ferguson, Green & Liebert (1984) found 19 sdB stars with main-sequence (MS) companions from the PG survey and derived a binary frequency of about 50 per cent. Allard et al. (1994) found 31 sdB binaries from 100 candidates chosen from the PG and KPD surveys and estimated that 54–66 per cent of sdB stars are in binaries with MS companions after taking selection effects into account. Thejll et al. (1995) and Ulla & Thejll (1998) also found that more than half of their sdB star candidates showed infrared flux excesses, indicating the presence of binary companions. Aznar Cuadrado & Jeffery (2001) obtained atmospheric parameters for 34 sdB stars from spectral energy distributions and found that 19 were binaries with MS companions, while 15 appeared to be single. These observations showed that at least half of the sdB stars were in binaries.

A major recent development has been the identification of many sdB stars as short-period binaries (Saffer, Livio & Yungelson 1998; Koen, Orosz & Wade 1998; Jeffery & Pollacco 1998; Wood & Saffer 1999; Orosz & Wade 1999; Moran et al. 1999; Maxted et al. 2000a; Maxted, Marsh & North 2000b; Maxted et al. 2001; Heber et al. 2002). In particular, Maxted et al. (2001) concluded that more than two-thirds of their candidates were binaries with short orbital periods from hours to days, and that most of the known companions were white dwarfs (WDs).

A variety of formation channels for sdB stars have been proposed in the past but mainly for single sdB stars because of the absence of identified sdB star binaries at the time. In the merger channel, two helium white dwarfs in a close binary are driven together by the orbital angular momentum loss due to gravitational wave radiation. When the white dwarfs merge and the merged object ignites helium, this produces a single sdB star (Webbink 1984; Iben & Tutukov 1986; Han 1998). Alternatively, stellar wind mass loss near the tip of the first giant branch (FGB) may strip off a giant's envelope and leave an almost bare helium core. If helium is ignited in the core, the star will appear as a single sdB star (D'Cruz et al. 1996). Sweigart (1997) has studied the evolution of globular-cluster stars and suggested that helium mixing driven by internal rotation substantially increases the helium abundance in the envelope; this may lead to enhanced mass loss along the FGB and the formation of an sdB star.

On the other hand, Mengel, Norris & Gross (1976) carried out conservative binary evolution calculations for a binary system with initial masses of 0.80 and 0.78 $M_\odot$ and a composition $X = 0.73$, $Z = 0.001$, and showed that there exists a range of initial separations for which stable mass transfer can produce an sdB star of $\sim$0.5 $M_\odot$ in a wide binary.

From a binary evolution point of view, these formation channels are not complete. When a star fills its Roche lobe near the tip of the FGB, mass transfer begins and may be dynamically unstable. This leads to the formation of a common envelope (CE) (Paczyński 1976), where the CE engulfs the helium core and the secondary. As a result of friction between the envelope and the immersed binary, the orbit shrinks, depositing a large amount of orbital energy in the envelope. If this energy is enough to eject the envelope and if helium is subsequently ignited in the core, an sdB star in a short-period binary is formed with a mass near 0.5 $M_\odot$. These are exactly the types of objects identified in large numbers by Maxted et al. (2001). If mass transfer near the tip of the FGB is dynamically stable, the envelope of the primary is lost as a result of stable RLOF, and the remnant core will be in a binary system with a long orbital period. It becomes an sdB star when helium in the primary's remnant is ignited. An additional channel for the formation of sdB stars in wide binaries, which has not received much attention in the past, involves binaries that experience stable RLOF when passing through the Hertzsprung gap (so-called early case B mass transfer) (Han, Tout & Eggleton 2000; Han et al., in preparation, hereafter Paper II). All of the sdB binaries produced through stable RLOF channels are consistent with the observations by Green, Liebert & Saffer (2000), who showed that some sdB stars appear to be members of long-period binaries.

The main purpose of this study is to re-examine the various scenarios for the formation of sdB stars in some detail. In this first paper, we concentrate on the individual evolutionary channels. Using detailed stellar and binary calculations, we model the physics and appearance of sdB stars and then test individual evolutionary channels using binary population synthesis (BPS). We demonstrate that all of the main evolutionary channels proposed previously can lead to the formation of sdB stars. As a byproduct we constrain the CE ejection efficiency from the observed period distribution of compact sdB binaries to arrive at a physically motivated and experimentally calibrated prescription for the CE phase.

The outline of this paper is as follows. In Section 2, we describe the stellar evolution code and the binary population synthesis code adopted in this study. In Section 3, we present the conditions for the formation of sdB stars from the CE ejection channel, their evolutionary tracks and simplified BPS models to constrain the CE ejection efficiency. In Section 4, we derive the conditions for helium ignition in objects that result from the merger of two He white dwarfs and use Monte Carlo simulations to determine their mass distribution. In Section 5, we investigate the criterion for stable RLOF and the formation of sdB stars in wide binaries. In the follow-up paper (Paper II) we will apply these results to a comprehensive binary population synthesis study and will estimate the relative importance of these individual channels.

2 THE STELLAR EVOLUTION AND THE BINARY POPULATION SYNTHESIS CODE

In this study, we employ two numerical computer codes: a stellar evolution code to determine the structure and to follow the evolution of sdB stars, and a binary population synthesis code to examine different evolutionary channels.

The stellar evolution code used is the one that was originally developed by Eggleton (1971, 1972, 1973), which has been updated with the latest input physics over the past three decades as described by Han, Podsiadlowski & Eggleton (1994, hereafter HPE) and Pols et al. (1995, 1998). The code distinguishes itself by the use of a self-adaptive non-Lagrangian mesh, the treatment of both convective

and semiconvective mixing as diffusion processes, and the simultaneous and implicit solution of both the stellar structure equations and the chemical composition equations, which includes convective mixing. These characteristics make the code very stable and easy to use. The current code uses an equation of state that includes pressure ionization and Coulomb interaction, recent opacity tables derived from Rogers & Iglesias (1992) and Alexander & Ferguson (1994a,b), nuclear reaction rates from Caughlan et al. (1985) and Caughlan & Fowler (1988), and neutrino loss rates from Itoh et al. (1989, 1992).

We set $\alpha = l/H_{\rm p}$, the ratio of the mixing length to the local pressure scaleheight, to 2. For Population I (Pop I) stars (with a typical composition of hydrogen abundance $X = 0.70$, helium abundance $Y = 0.28$ and metallicity $Z = 0.02$), such a value for α gives a roughly correct lower main sequence, as determined observationally by Andersen (1991). It also well reproduces the location of the red giant branch in the Hertzsprung–Russell (HR) diagram for stars in the Hyades supercluster (Eggen 1985), as determined by Bessell et al. (1989). A fit to the Sun also leads to $\alpha = 2$ as the most appropriate choice (Pols et al. 1998).

For convective overshooting, the code does not employ a prescription in terms of the pressure scaleheight $H_{\rm p}$ where the overshooting length is a fixed fraction of $H_{\rm p}$. Instead, the code uses an approach based on the stability criterion itself, the '$\delta_{\rm ov}$ prescription', by incorporating a condition that mixing occurs in a region with

$$\nabla_{\rm r} > \nabla_{\rm a} - \delta_{\rm ov}/(2.5 + 20\zeta + 16\zeta^2),$$

where ζ is the ratio of radiation pressure to gas pressure and $\delta_{\rm ov}$ is a specified constant, the overshooting model parameter. Critical tests of stellar evolution by means of double-lined eclipsing binaries (Schröder, Pols & Eggleton 1997; Pols et al. 1997) show that $\delta_{\rm ov} = 0.12$ gives the best fit to the observed systems, where $\delta_{\rm ov} = 0.12$ corresponds to an overshooting length of $\sim$0.25 pressure scaleheights.

Roche lobe overflow is treated directly within the code. It has been tested thoroughly and works very reliably. Because the mesh spacing is computed along with the structure, the inclusion of RLOF is almost trivial: it just requires a modification of one surface boundary condition. The boundary condition is written as

$$\frac{{\rm d}m}{{\rm d}t} = C\,{\rm Max}\left[0, \left(\frac{r_{\rm star}}{r_{\rm lobe}} - 1\right)^3\right], \qquad (1)$$

where ${\rm d}m/{\rm d}t$ gives the rate at which the mass of the star changes, $r_{\rm star}$ is the radius of the star, and $r_{\rm lobe}$ is the radius of its Roche lobe. C is a constant. With $C = 1000\,{\rm M}_\odot\,{\rm yr}^{-1}$, RLOF proceeds steadily, and the lobe-filling star overfills its Roche lobe as necessary but never overfills its lobe by a substantial amount [typically $(r_{\rm star}/r_{\rm lobe} - 1) \lesssim 0.001$].

The stellar evolution code described above evolves only a single star or both components of a binary at a time. However, stellar evolution theory should give and predict the *statistical* properties of a whole stellar population as well as the properties of individual stars or binaries. In order to investigate statistical properties of stars and check evolutionary mechanisms for different types of stars, Han, Podsiadlowski & Eggleton (1995a) developed a Monte Carlo simulation code, or 'binary population synthesis' (BPS) code, which is able to evolve a sample of one million or more stars (including binaries) simultaneously by interpolating the properties of individual stars as a function of evolutionary age in a specially prepared grid of stellar models. This code has been steadily updated ever since (Han 1995; Han et al. 1995b; Han 1998; Han et al. 2001).

The BPS code needs a grid of stellar evolution models. Taking Pop I as the standard population model, we carried out a large number of stellar evolution calculations for a wide range of masses (0.08 to 126 $M_\odot$), including the evolution of helium stars from 0.32 to 8 $M_\odot$, at an interval of $\sim$0.1 in $\log M$. In the calculation of the stellar models, we did not include stellar wind mass loss for most of the grids calculated. However, for massive stars the evolution was terminated at the Humphreys–Davidson (HD) limit (Humphreys & Davidson 1979; Lamers & Fitzpatrick 1988; Fitzpatrick & Garmany 1990; Ulmer & Fitzpatrick 1998); we assumed that at the HD limit the envelope of the massive star was lost completely, and then treated the remnant core as a helium star. The evolution of low- and intermediate-mass stars was terminated at the point when the total energy of the envelope became positive, assuming that the envelope was ejected at this point, leaving a white dwarf remnant (see HPE). For a given star we obtain the required stellar parameters at a particular evolutionary age (e.g. the luminosity, effective temperature, radius, core mass, core radius, envelope binding energy) by interpolation from our set of stellar evolutionary tracks.

In BPS, one has to evolve binaries as well as single stars. At present stellar wind mass loss and binary interactions are included in the form of simple prescriptions. We plan to replace these by ever more realistic modelling as part of our ongoing work. One important improvement we have implemented in the present work is that we adopted full binary evolution calculations for systems where RLOF occurs in the Hertzsprung gap (Han et al. 2000). Another uncertainty that we will address in more detail in the future is the criterion for dynamically unstable RLOF. If the primary fills its Roche lobe as a red giant, RLOF may be dynamically unstable if the mass ratio at the onset is larger than some critical value $q_{\rm c}$, given e.g. by Hjellming & Webbink (1987) and Webbink (1988). However, this critical mass ratio only applies to conservative RLOF and does not fully take into account the detailed dynamics at the onset of mass transfer. From observations it is clear that RLOF on the first giant branch/asymptotic giant branch (FGB/AGB) is non-conservative (Giannuzzi 1981; Shore 1988). Part of the transferred mass is lost from the system. In our model we assume that the lost matter carries away the same specific angular momentum as pertains to the system. Defining a mass transfer efficiency, $\alpha_{\rm RLOF}$, as the ratio of the mass accreted by the secondary to the mass transferred from the primary ($\alpha_{\rm RLOF} = 1$ for conservative RLOF), we find that the critical ratio $q_{\rm c}$ depends strongly on the mass transfer efficiency (Han et al. 2001). Dynamically unstable mass transfer may result in the formation of a common envelope (CE) (Paczyński 1976), leading either to the formation of a close binary or the complete merger of the two components (see Section 3).

Given a binary sample, the BPS code performs all the necessary interpolations in the model grid, integrates the mass loss along evolutionary tracks for an assumed stellar wind law, and deals with all the binary interactions. The output of the code are all the parameters for different types of binaries or single objects formed as a consequence of the evolution and various interactions.

In the original version, the BPS code used the following stellar model grids as input:

(i) $Z = 0.02$, no stellar wind, with no overshooting, 0.08–126.0 $M_\odot$ for normal stars ($X = 0.70$ and $Y = 0.28$), 0.32–8.0 $M_\odot$ for helium stars.

(ii) $Z = 0.004$, no stellar wind, with no overshooting, 0.1–126.0 $M_\odot$ for normal stars ($X = 0.74$ and $Y = 0.256$), 0.32–8.0 $M_\odot$ for helium stars.

(iii) $Z = 0.001$, no stellar wind, with no overshooting, 0.1–126.0 $M_\odot$ for normal stars ($X = 0.75$ and $Y = 0.249$), 0.32–8.0 $M_\odot$ for helium stars.

For the purpose of this paper, we have also calculated several additional grids that include convective overshooting and stellar wind mass loss:

(i) $Z = 0.02$, no stellar wind, but with overshooting, 0.63–3.2 $M_\odot$ for normal stars.
(ii) $Z = 0.02$, 1/4 Reimers' wind (Reimers 1975), and with overshooting, 0.63–3.2 $M_\odot$ for normal stars.
(iii) $Z = 0.02$, 1/4 Reimers' wind, but without overshooting, 0.63–3.2 $M_\odot$ for normal stars.
(iv) $Z = 0.02$, 1/2 Reimers' wind, and with overshooting, 0.63–3.2 $M_\odot$ for normal stars.
(v) $Z = 0.02$, 1/2 Reimers' wind, but without overshooting, 0.63–3.2 $M_\odot$ for normal stars.
(vi) $Z = 0.004$, 1/4 Reimers' wind, and with overshooting, 0.63–3.2 $M_\odot$ for normal stars.

3 THE COMMON-ENVELOPE CHANNEL

In the common-envelope (CE) channel, the sdB star forms in a close binary as a consequence of dynamical mass transfer and a CE phase where the progenitor, a giant star, starts to fill its Roche lobe when it is relatively close to the tip of the first giant branch (FGB). This situation generally occurs when the radius of the mass-losing star increases faster than its Roche lobe radius. This leads to mass transfer on a dynamical time-scale and the formation of a common envelope where the envelope of the giant engulfs both its degenerate core and the companion star. Friction between these orbiting components and the envelope causes the orbit of the immersed binary to shrink. If the orbital energy released in the process is able to eject the envelope, this process leaves a very tight binary consisting of the degenerate core of the giant and the companion star. This is believed to be the main mechanism, originally proposed by Paczyński (1976), by which an initially wide binary is transformed into a very close system. If this happens when the giant was sufficiently close to the tip of the FGB at the beginning of mass transfer, i.e. the core was close to experiencing the helium flash, the remnant core of the giant may still ignite helium (as first demonstrated by Castellani & Castellani 1993) and hence become a helium-core-burning sdB star, where the companion can be either a white dwarf (WD) or in some cases a low-mass star. These are exactly the objects observed in large numbers by Maxted et al. (2001). Note that the companion star can in principle also be a normal dwarf star with a mass as high as 1–2 $M_\odot$ (which depends on the condition for dynamical mass transfer; see Section 5.1). However, such a system would have a composite spectrum. Since such systems were excluded from the PG catalogue, they would not appear in radial-velocity studies based on this catalogue.

The details of CE evolution, in particular the conditions for which the envelope can be ejected, are far from well understood at the present time (see e.g. Iben & Livio 1993). On the other hand, the identification of a large number of sdB stars in very close binaries, which must all have passed through such a well-defined evolutionary channel, provides a unique opportunity to test particular models of CE evolution and may even help to calibrate the criterion for CE ejection. Indeed, it is one of the surprises of the observations by Maxted et al. (2001) that the period distribution is extremely wide, ranging from 2 h to more than ∼10 d.

3.1 The minimum core mass for helium ignition

In order for the degenerate core to ignite helium in a helium flash after the envelope has been ejected, its giant progenitor had to be relatively close to the tip of the FGB at the beginning of mass transfer. D'Cruz et al. (1996) have shown by varying the wind mass-loss rate on the FGB that the core mass for helium ignition can be as low as 0.45 $M_\odot$. The situation considered here is slightly different since mass ejection in a CE phase is a sudden event, occurring on a time-scale short compared to the evolutionary time-scale of a giant. We therefore performed a comprehensive series of stellar calculations where we assumed that a giant loses its hydrogen-rich envelope near the tip of the FGB to determine the minimum core mass above which the core will still ignite helium after the ejection of the envelope. This critical mass generally depends on the zero-age main sequence (ZAMS) mass of the giant, but also on the assumptions about mass loss, metallicity and the degree of convective overshooting from the core. To examine these various situations, we therefore considered three sets of calculations. Set (1) assumes no stellar wind, no convective overshooting and a solar metallicity of $Z = 0.02$. In set (2) we again use a solar metallicity, but also include a stellar wind parametrized by a Reimers' wind mass-loss law

$$\dot{M}_{\rm wind} = 4 \times 10^{-13} \eta RL/M, \qquad (2)$$

where for the standard model we use an efficiency $\eta = 1/4$ (Renzini 1981; Iben & Renzini 1983; Carraro et al. 1996). In this set, we also take into account convective overshooting based on the calibration of this parameter by Schröder et al. (1997) and Pols et al. (1997), which corresponds to overshooting of ∼0.25 pressure scaleheights from the core. Set (3) is similar to set (2) except that we use a metallicity of $Z = 0.004$, characteristic of a thick disc population (Gilmore, Wyse & Kuijken 1989).

We find that the maximum initial ZAMS mass below which stars experience a helium flash decreases from 2.25 $M_\odot$ for set (1) to 1.99 $M_\odot$ for set (2) and 1.8 $M_\odot$ in set (3). Stars with ZAMS masses larger than these values ignite helium non-degenerately. Some of these can also become sdB stars.

To determine the minimum core mass for the helium flash for each ZAMS mass, we considered a series of models near the tip of the FGB and took the H-rich envelopes off at a high rate (chosen to be 10^{-3} $M_\odot$ yr^{-1} times the mass of the star in solar units) until the envelopes collapsed (note that we switched hydrogen burning off when the envelope mass became less than 0.002 $M_\odot$ to prevent the occurrence of hydrogen shell flashes). We then followed the subsequent evolution of the core either until it had cooled to a surface temperature of less than 5000 K or until it ignited helium in the core. In Table 1 and Fig. 1 we present the minimum core mass as a function of ZAMS mass above which helium is ignited and also the core mass at the tip of the FGB. These results show that the minimum core mass has to be typically within 5 per cent of the core mass at the tip of the FGB where the minimum decreases from 0.45/0.46 $M_\odot$ for the less massive progenitors to 0.39/0.40 $M_\odot$ for the most massive stars that still experience a helium flash. While the range in mass is relatively small, it corresponds to a fairly large range (∼15 per cent) in radius (also shown in Table 1), since giants expand quite significantly close to the tip of the FGB.

Note that the more massive stars do not experience a helium flash. If the envelopes are stripped off near the tip of the FGB for stars with $2.05 \leqslant M_0 \leqslant 2.265\,M_\odot$ (set 2, Pop I) or with $1.85 \leqslant M_0 \leqslant 2.0\,M_\odot$ (set 3, $Z = 0.04$), the cores ignite helium under non-degenerate conditions (as shown in Table 1 and Fig. 1). For even more massive stars, the cores will burn helium even when

Table 1. The minimum core mass for the helium flash/helium ignition.[a]

$\frac{M_0}{M_\odot}$	$\frac{M_c^{min}}{M_\odot}$	$\frac{M_c^{tip}}{M_\odot}$	$\log\left(\frac{R^{min}}{R_\odot}\right)$	$\log\left(\frac{R^{tip}}{R_\odot}\right)$
No wind, no overshooting, $Z = 0.02$				
0.794	0.4529	0.4742	2.2245	2.2923
1.000	0.4502	0.4725	2.1838	2.2539
1.259	0.4492	0.4720	2.1492	2.2161
1.585	0.4461	0.4699	2.1069	2.1772
1.995	0.4174	0.4422	1.9537	2.0453
2.114	0.4010	0.4217	1.8628	1.9532
Reimers' wind ($\eta = 1/4$), with overshooting, $Z = 0.02$				
0.800	0.4538	0.4746	2.2482	2.3076
1.000	0.4509	0.4727	2.1985	2.2707
1.260	0.4496	0.4723	2.1578	2.2264
1.600	0.4351	0.4601	2.0656	2.1465
1.900	0.3889	0.4087	1.8113	1.9050
Helium ignited non-degenerately				
2.050	0.3190	0.3224	1.4290	1.4355
2.265	0.3181	0.3460	1.2881	1.5317
2.512	0.3223	0.3715	0.6871	1.5612
3.162	0.4385	0.4669	0.7489	1.6891
3.981	0.5947	0.6146	0.8068	1.8685
5.012	0.8049	0.8286	0.8598	2.0618
6.310	1.1108	1.1284	0.9181	2.2587
Reimers' wind ($\eta = 1/4$), with overshooting, $Z = 0.004$				
0.800	0.4642	0.4855	2.0886	2.1475
1.000	0.4604	0.4826	2.0530	2.1184
1.260	0.4578	0.4810	2.0186	2.0856
1.600	0.4314	0.4564	1.8829	1.9710
1.750	0.3933	0.4149	1.6800	1.7825
Helium ignited non-degenerately				
1.850	0.3238	0.3367	1.4003	1.4439
2.000	0.3175	0.3403	1.2903	1.4594
2.512	0.3381	0.3935	0.5740	1.5122
3.162	0.4492	0.4942	0.6343	1.6480
3.981	0.6006	0.6398	0.6910	1.8080
5.012	0.8143	0.8579	0.7515	1.9889
6.310	1.1187	1.1539	0.8126	2.1707

[a] $M_0 =$ initial zero-age main-sequence mass; $M_c^{min} =$ minimum mass of the He core for helium ignition; $M_c^{tip} =$ mass of the He core at the tip of the first giant branch; $R^{min} =$ stellar radius corresponding to M_c^{min}; $R^{tip} =$ the radius at the tip of the first giant branch. The models were calculated by taking off mass from the envelope at a rate of 10^{-3} $M_\odot$ yr^{-1} times the mass of the star in solar units until the envelope collapsed. Note, however, that M_c^{min} and R^{min} for $M_0 \geqslant 2.5\,M_\odot$ correspond to models at the end of the main sequence, while those with $M_0 < 2.5\,M_\odot$ are models on the FGB.

the envelopes are lost in the Hertzsprung gap. The envelopes of these massive stars are generally much more tightly bound than those near the tip of the FGB for stars with degenerate cores and hence are much harder to eject. Generally, the more massive the star, the more tightly bound is its envelope. Therefore we find in the BPS calculations that CE ejection is only possible for stars that are not too massive. These, however, leave fairly low-mass sdB stars ($\sim$0.35 $M_\odot$) with very short orbital periods.

3.2 Evolutionary tracks of sdB stars

Since helium ignition in a degenerate core causes a mild thermonuclear runaway which leads to the expansion of the core on a dynamical time-scale, we are unable to follow it with our hydrostatic stellar evolution code. However, once the core has expanded sufficiently and the core has become non-degenerate, helium burning quickly stabilizes and the core regains hydrostatic equilibrium. In Figs 2 and 3 we show the subsequent evolution of various sdB stars in a T_{eff}–log g diagram and a standard Hertzsprung–Russell (HR) diagram. The T_{eff}–log g plot is particularly useful, since sdB stars can be placed on it based on their spectra alone with the help of model stellar atmospheres independent of their distance and their luminosity. The initial models (i.e. on the zero-age horizontal branch, ZAHB) in Figs 2(a)–(c) were constructed in such a way that they had the same core mass and chemical composition as the appropriate models from set (2) in Section 3.1 at the point of helium ignition (i.e. at the helium flash).

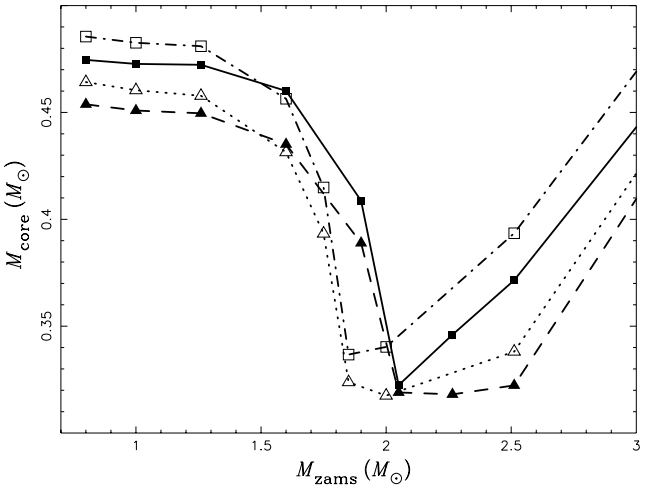

Figure 1. Range of core masses for the occurrence of a He flash (or non-degenerate helium ignition) as a function of initial mass for $Z = 0.02$ (dashed and solid curves) and $Z = 0.004$ (dotted and dot-dashed curves). The lower curve for each set gives the minimum core mass above which a star burns helium, and the upper curve gives the core mass at the normal tip of the first giant branch (FGB).

Fig. 2(a) shows the evolution of various selected sdB models with different total masses, originating from a range of progenitor masses and with a variety of different envelope masses. The symbols give the position of observed sdB stars [from Maxted et al. (2001); note, however, that the uncertainties in log g are about 0.15; see Saffer et al. (1994)], where the different symbols either correspond to different ranges of orbital periods (if known; filled symbols) or indicate the magnitude of radial velocity variations for systems without known orbital periods (open symbols). As the figure shows, there is generally excellent overlap between the evolutionary tracks and the observed systems.

To show this more systematically, Fig. 2(b) presents the tracks for sdB stars of a typical mass of 0.46 $M_\odot$, but with different masses of the hydrogen-rich envelope, ranging from 0 to 0.01 $M_\odot$ (here the envelope is defined as the outer part of the sdB star with a hydrogen mass fraction larger than 0.01). The two dashed curves give the location of the ZAHB (right curve) and the location where the sdB stars exhaust helium in their cens (left curve). Thin crosses are also shown along the tracks to indicate the speed of evolution across the diagram. As one would expect, sdB stars without hydrogen envelopes are the hottest and the most compact, and the evolutionary tracks are shifted towards lower temperatures and lower gravity as the mass in the hydrogen-rich envelope is increased. The majority of observed systems lie between the dashed curves, marking the range of helium-core-burning objects. There appears

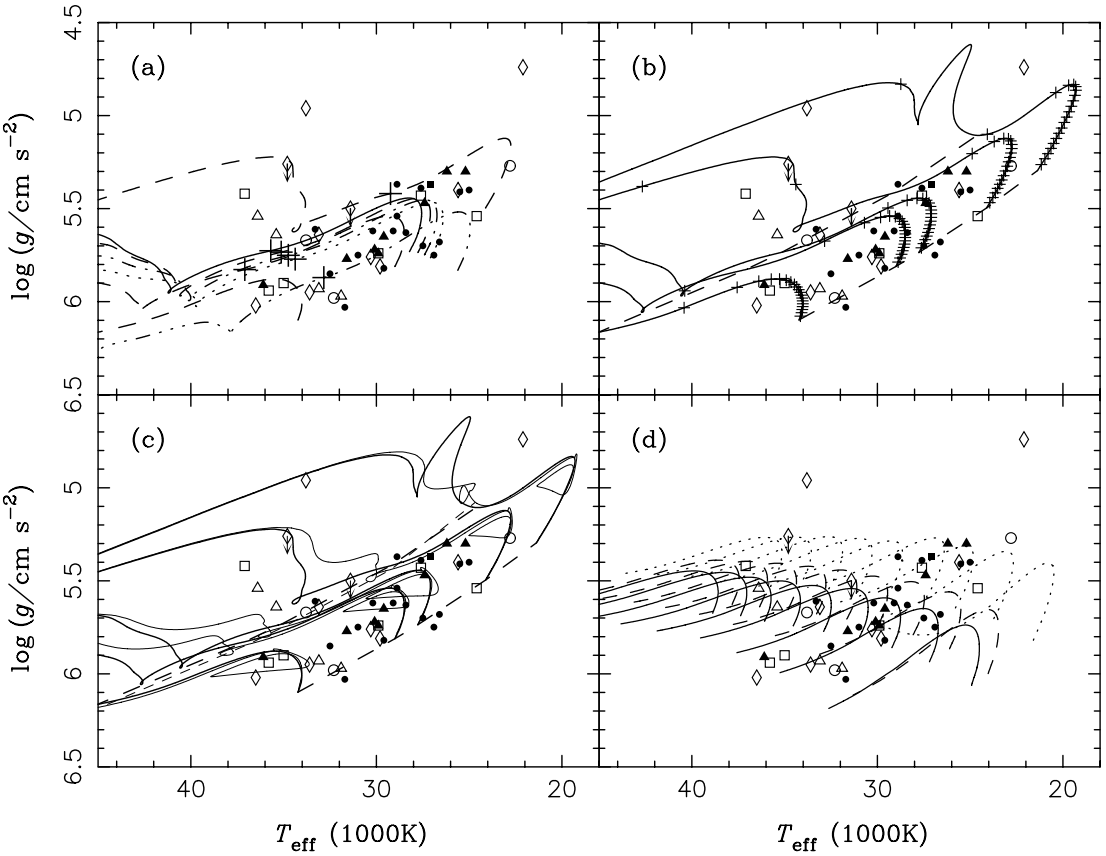

Figure 2. Evolutionary tracks of sdB stars in the $T_{\rm eff}$–log g diagram. Filled circles show the position of observed sdB stars with orbital periods $P_{\rm orb} < 1$ d, solid triangles are for systems with period $1 < P_{\rm orb} < 10$ d and solid squares for systems with $P_{\rm orb} > 10$ d. Circles show systems that have radial velocity variations $\mathrm{d}V > 40$ km s^{-1}, triangles are for systems with $20 < \mathrm{d}V < 40$ km s^{-1}, squares for $10 < \mathrm{d}V < 20$ km s^{-1} and diamonds for $\mathrm{d}V < 10$ km s^{-1}, where $\mathrm{d}V$ is the maximum difference between radial velocities measured for a particular object. Arrows indicate lower limits for g. (a) Tracks for eight selected models (Pop I, Reimers' wind with $\eta = 1/4$ and convective overshooting). The solid curve is for a ZAMS model of 0.8 $M_\odot$ and an sdB of 0.47 $M_\odot$ with an envelope mass of 0.002 $M_\odot$. The dashed curves are for a ZAMS model of 1.00 $M_\odot$ and an sdB mass of 0.46 $M_\odot$ but with decreasing envelope masses (top to bottom: 0.005, 0.002, 0.001 and 0.000 $M_\odot$, respectively). The dot-dashed curve is for a ZAMS mass of 1.26 $M_\odot$, an sdB mass of 0.45 $M_\odot$ and an envelope mass of 0.002 $M_\odot$. The dotted curve is for a ZAMS mass of 1.60 $M_\odot$, an sdB mass of 0.44 $M_\odot$ and an envelope mass of 0.002 $M_\odot$. The triple dot-dashed curve is for a ZAMS mass of 1.90 $M_\odot$, an sdB mass of 0.40 $M_\odot$ and an envelope mass of 0.002 $M_\odot$. Crosses show the point of central He exhaustion. (b) The dependence of the evolutionary tracks on the envelope mass. All models are for a ZAMS model of 1 $M_\odot$ and an sdB mass of 0.46 $M_\odot$ (for Pop I, Reimers' wind with $\eta = 1/4$ and with convective overshooting). The solid curves from bottom to top are for envelope masses of 0.000, 0.001, 0.002, 0.005, 0.010 $M_\odot$, respectively. The left-hand dashed curve indicates the point of central helium exhaustion, while the right-haand dashed curve shows the locus of ZAHB models. The age differences between adjacent crosses are 10^7 yr. (c) The dependence of evolutionary tracks on convective overshooting. The thin solid/dashed curves do not include convective overshooting, while the solid ones do [the latter are the same as in (b)]. (d) The variation with sdB mass (for $Z = 0.02$, with overshooting). Solid curves are for an envelope mass of 0.001 $M_\odot$, dashed curves for 0.002 $M_\odot$ and dotted curves for 0.005 $M_\odot$. For each set, the curves from right to left are for sdB masses of 0.35, 0.40, 0.45, 0.50, 0.55, 0.60, 0.65, 0.70, 0.75 $M_\odot$, respectively. All curves show the tracks from the ZAHB to the point of central helium exhaustion.

to be, however, a fairly large range of envelope masses from 0 to $\sim$0.005 $M_\odot$. There are also a few objects that lie significantly outside the helium-core-burning band. While evolutionary tracks will pass through most of these observational points after the end of helium core burning, this corresponds to a fast evolutionary phase, as can be seen from the wide separation of thin crosses. A more likely explanation is that some of these are more massive objects.

In Fig. 2(c) we show the dependence of evolutionary tracks of sdB stars on convective overshooting. The sdB stars without convective overshooting display 'breathing pulses' (see e.g. Castellani et al. 1985).

Fig. 2(d) shows the dependence of the location of the helium-core-burning sdB stars on the mass of the sdB star for three envelope masses (0.001, 0.002, 0.005 $M_\odot$). The masses of the sdB stars range from 0.35 to 0.75 $M_\odot$ (note that sdB stars more massive than $\sim$0.5 $M_\odot$ can form in some of the other evolutionary channels discussed later in this paper).[1] Four of the six objects that were outside the helium-core-burning band in Fig. 2(b) fall on to a helium-core-burning track with a more massive sdB star. This may provide an indication that some of the sdB stars have masses as high as 0.7 $M_\odot$. The two remaining objects (PG 1553+273 and PG 1051+501), both of which show low radial velocity variations, lie well above all of these tracks. This suggests that they have either substantially more massive envelopes (see Section 5) or have already exhausted

[1] Unlike the previous models, the composition profiles for the ZAHB models were taken from a 3.2 $M_\odot$ helium-core-burning star that was artificially transformed into an sdB star of the chosen total mass and envelope mass.

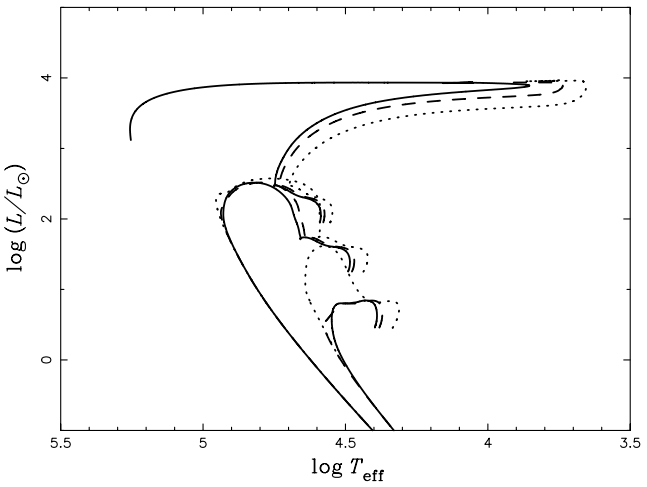

Figure 3. HR diagram of sdB stars. Solid curves are for envelope masses of 0.001 $M_\odot$, dashed curves for 0.002 $M_\odot$ and dotted curves for 0.005 $M_\odot$, respectively. For each set, the curves from bottom to top are for sdB masses of 0.35, 0.50, 0.75 $M_\odot$, respectively. Note that the composition profiles were not taken from helium flash models, but were constructed from a 3.2 $M_\odot$ Pop I star burning helium smoothly. The sdB model for the 0.75 $M_\odot$ star was terminated when it experienced a hydrogen shell flash.

helium in their cores and are now evolving quickly away from the horizontal branch.

3.3 Common-envelope ejection

CE evolution is one of the most important but also one of the least understood phases of binary evolution – see Iben & Livio (1993), Taam & Sandquist (2000) and Podsiadlowski (2001) for reviews with different emphasis. One of the uncertainties is related to the conditions under which a binary experiences dynamical mass transfer and a CE phase (this will be further discussed in Section 5.1). A second area of uncertainty is related to the criterion for the ejection of the CE, which crucially determines the orbital period distribution of post-CE binaries. The latter depends on what fraction of the orbital energy that is released in the spiral-in process can be used to drive the ejection, which depends on the efficiency with which energy can be transported to the stellar surface where it can be radiated away. It also depends on the efficiency of the dynamics of the ejection process; e.g. if the envelope is ejected with a velocity much larger than the surface escape velocity, the efficiency per unit mass will be reduced (see e.g. the discussion in Taam & Sandquist 2000). A further factor is related to the question of what fraction of the thermal energy, in particular the ionization energy, can be converted into kinetic energy and can help to drive the expansion of the envelope. This is particularly important for giants that fill their Roche lobes near the tip of the FGB or the AGB, since in such extended stars the total binding energy of the envelope, including the ionization energy, is greatly reduced and ultimately becomes zero (see HPE). This has the consequence that very little spiral-in is required to release, in principle, enough energy to eject these loosely bound envelopes; this leads to post-CE binaries with relatively long orbital periods.

In binary population synthesis (BPS) studies it is commonly assumed that the common envelope is ejected when the change in orbital energy times some efficiency factor, $\alpha_{\rm CE}$, exceeds the binding energy of the envelope, where the latter is often approximated by a simple analytical expression. Our approach is rather different from this and it is designed to provide a more physical parametrization of the CE ejection process. Our common-envelope ejection criterion can be written as

$$\alpha_{\rm CE}|\Delta E_{\rm orb}| > |E_{\rm gr} + \alpha_{\rm th} E_{\rm th}|. \quad (3)$$

The left-hand side represents the fraction of the change in the orbital energy that can be used for the ejection, as in most other commonly used prescriptions. However, on the right-hand side, we include both the gravitational energy of the envelope ($E_{\rm gr}$) and a fraction $\alpha_{\rm th}$ of its thermal energy ($E_{\rm th}$), which in particular includes the ionization energy. Moreover, instead of using analytical approximations for these energies, we use the values obtained from full stellar structure calculations (see HPE for details and also Dewi & Tauris 2000). The fact that we have two parameters, $\alpha_{\rm CE}$ and $\alpha_{\rm th}$, instead of one allows us to specifically assess the importance of the thermal energy contribution. Indeed, the observations of post-CE sdB binaries from this well-defined evolutionary channel may allow the calibration of this parameter – at least in principle.

3.4 A simplified BPS model

In order to test the CE ejection criterion, we need to perform a binary population study where we simulate the period distribution of sdB binaries after the ejection of the common envelope. To avoid unnecessary complications, we use a simplified BPS model in this section, simplified in the sense that we do not model the evolution of the system before the CE phase that leads to the formation of the close sdB binary. We also restrict ourselves to systems where the companion star is likely to be a white dwarf (WD). The model is completely specified by three distributions: the distribution of the white-dwarf mass, the mass of the giant, and the orbital separation before the CE phase. We use a uniform distribution in $\log(a/{\rm R}_\odot)$ from 1 to 4 where a is the orbital separation, a simple WD mass distribution [$f(M_{\rm WD}) = \frac{10}{3}\,{\rm M}_\odot^{-1}$ for $0.25 < M_{\rm WD}/{\rm M}_\odot < 0.45$ or $0.55 < M_{\rm WD}/{\rm M}_\odot < 0.65$] and a Miller & Scalo (1979) mass distribution for the giant between 0.8 and 8 $M_\odot$. The WD mass distribution may seem a little bit odd at first sight, but it actually mimics the bimodal mass distribution of WDs after the first RLOF phase as found in previous BPS studies (Han 1995, 1998; Han et al. 1995a,b, 2001). We emphasize that because of the wide distribution in $\log a$, it is almost certain that the resulting orbital period distribution of post-CE sdB binaries will be wider than what would be obtained in a more realistic simulation, since in a full BPS simulation only a subset of this parameter space would be realized by actual systems (see Paper II). Nevertheless, as we shall show below, this method still provides a good diagnostic for the CE efficiency.

3.4.1 Population I BPS simulations

In our first series of BPS simulations, we assume a Population I metallicity of $Z = 0.02$ and include convective overshooting (of 0.25 pressure scaleheights). We consider three sets of stellar models: (1) models with no stellar wind; (2) models with a Reimers wind mass loss with $\eta = 1/4$; and (3) models with a Reimers wind with $\eta = 1/2$. For each of these three sets we take six combinations of CE parameters $\alpha_{\rm CE}$ and $\alpha_{\rm th}$, including both efficient and inefficient models.

(a) $\alpha_{\rm CE} = 0.2$, $\alpha_{\rm th} = 0.0$;
(b) $\alpha_{\rm CE} = 0.5$, $\alpha_{\rm th} = 0.0$;
(c) $\alpha_{\rm CE} = 0.5$, $\alpha_{\rm th} = 0.5$;
(d) $\alpha_{\rm CE} = 0.75$, $\alpha_{\rm th} = 0.75$;

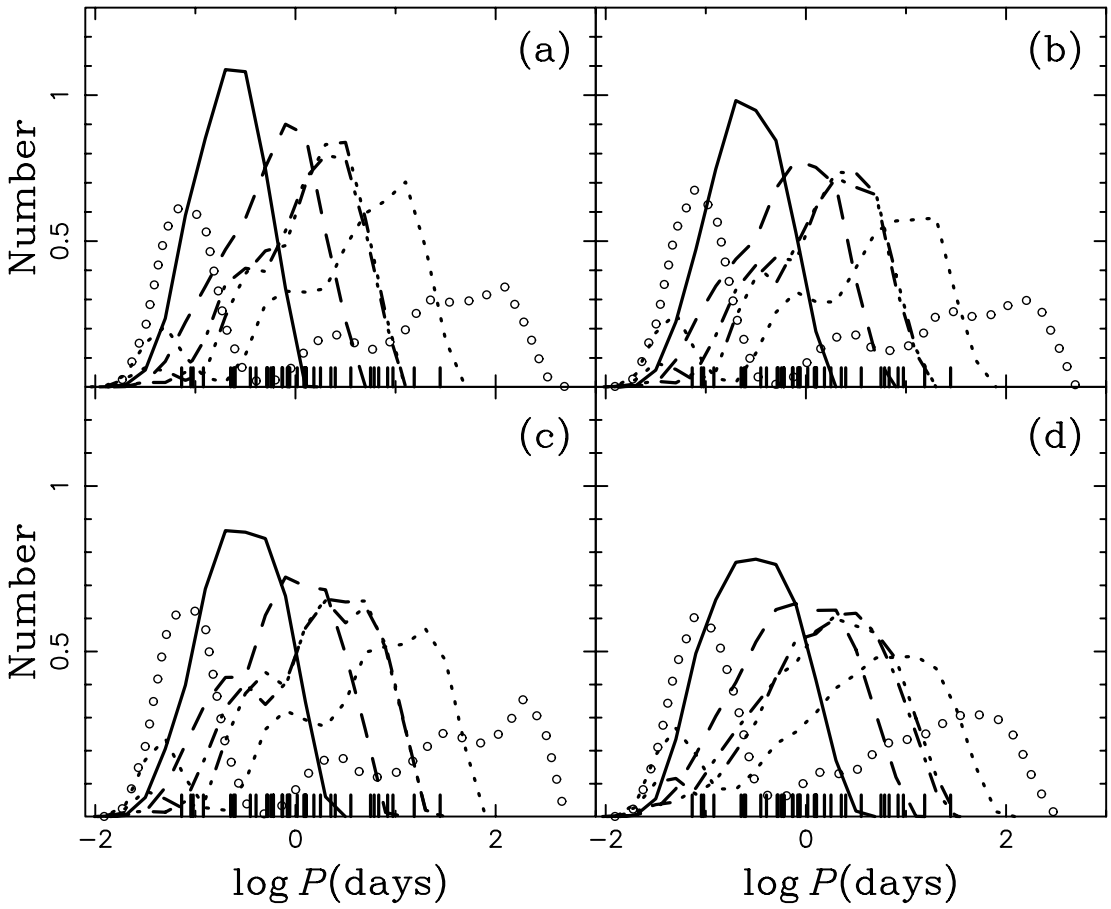

Figure 4. Orbital-period distributions for post-CE sdB stars. Panels (a), (b) and (c) are for Pop I metallicity, corresponding to stellar models with Reimers coefficient $\eta = 0$, 1/4, 1/2 respectively. Panel (d) is for $Z = 0.004$. In each panel, the distribution represented by solid, dashed, dot-dashed, dotted, triple dot-dashed curves, and circle symbols correspond to combinations (a) to (f) for the CE ejection parameters $\alpha_{\rm CE}$ and $\alpha_{\rm th}$. Note that the dot-dashed and triple dot-dashed curves almost overlap completely. The short ticks along the period axis indicate the position of observed systems (systems with dM companions, e.g. PG 1336 − 018, HW Vir and HS 0705 + 6700, are not included).

(e) $\alpha_{\rm CE} = 1.0$, $\alpha_{\rm th} = 0.0$;
(f) $\alpha_{\rm CE} = 1.0$, $\alpha_{\rm th} = 1.0$.

The resulting post-CE orbital period distributions for these three sets are shown in Figs 4(a)–(c). First, note by comparing the three panels that the different assumptions about the stellar wind make relatively little difference. On the other hand, the variation of the CE parameters affects the orbital period distributions quite dramatically. The overall behaviour of the various curves is relatively easy to understand.

In the case of inefficient CE ejection, i.e. low $\alpha_{\rm CE}$, the binary has to spiral in much further during the CE phase before enough energy has been deposited in the envelope to make ejection possible, resulting in very short orbital periods. As $\alpha_{\rm CE}$ is increased, the orbital period distribution shifts towards longer orbital periods. Increasing the value of $\alpha_{\rm th}$ also increases the post-CE orbital periods, since it reduces the binding energy of the envelope. It also widens the period distribution very substantially. This reflects the relative importance of the ionization energy, which varies significantly between a star of 1 $M_\odot$ and 1.9 $M_\odot$. For a 1 $M_\odot$ star, the total binding energy of the envelope near the tip of the FGB is close to zero (in fact, it may be positive, see HPE), implying that the envelope is only very loosely bound and that very little spiral-in is required to eject it. On the other hand, the envelope of a 1.9 $M_\odot$ star is much more tightly bound, leading to much smaller post-CE orbital periods of the systems. Some of the curves (e.g. the dotted ones) have three peaks. The left one corresponds to giants with $M_0 \gtrsim 2\,M_\odot$ which have much more tightly bound envelopes than FGB stars with $M_0 \lesssim 1.99\,M_\odot$. Since this requires much deeper spiral-in before the envelope can be ejected, it leads to the shortest orbital periods. The middle and the right peaks are the result of CE ejections for FGB stars with $M_0 \lesssim 1.99\,M_\odot$, where the middle peak corresponds to white dwarf primaries with $0.25 \leqslant M_{\rm WD} \leqslant 0.45\,M_\odot$ and the right peaks to white dwarfs with $0.55 \leqslant M_{\rm WD} \leqslant 0.65\,M_\odot$. In cases where the CE ejection is not very efficient, i.e. either $\alpha_{\rm CE}$ or $\alpha_{\rm th}$ is small, the differences in the period distributions for the two sets of white dwarfs tend to be small and the latter two peaks tend to merge into one.

The short ticks in these panels along the orbital period axis show the periods of sdB binaries with known orbital periods (Maxted et al. 2001). As is clear by inspection, the simulated period distributions taken together cover the whole range of observed periods, although no single model on its own provides a perfect fit to the observed distribution. The best models require high values for both $\alpha_{\rm CE}$ and $\alpha_{\rm th}$ in order to cover the whole range of orbital periods. Inspection of Figs 4(a)–(c) suggests that the dotted simulations with $\alpha_{\rm CE} = \alpha_{\rm th} = 0.75$ provide the best overall representation of the observed period distribution. Such a combination of parameters is

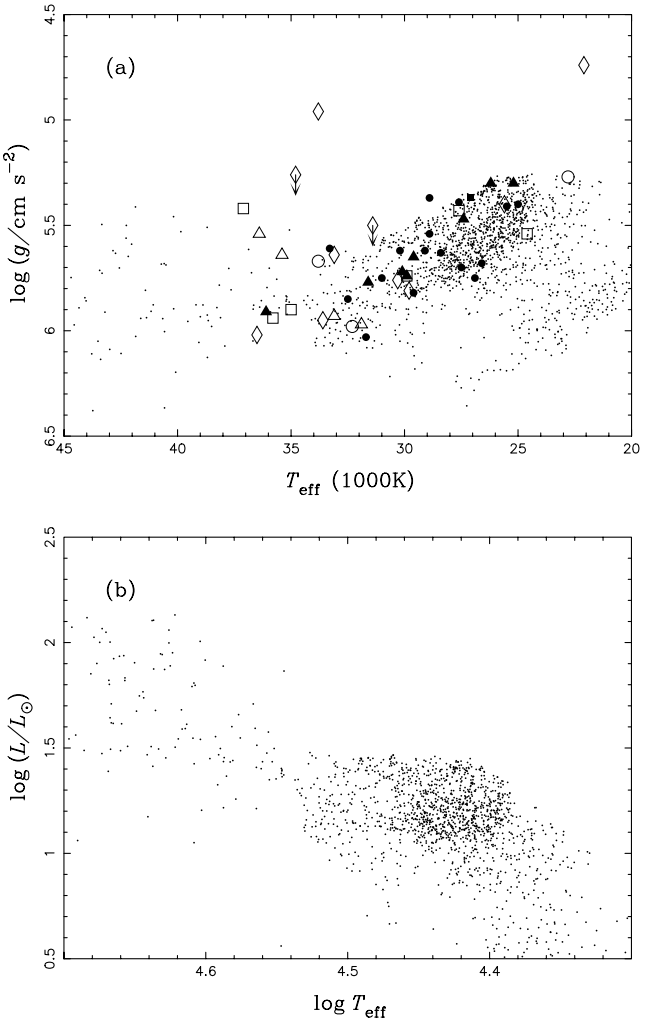

Figure 5. Simulated distribution in the $T_{\rm eff}$–log g (top panel) and HR diagram (bottom panel) for a 'reasonable' model with $\alpha_{\rm CE} = \alpha_{\rm th} = 0.75$ (dotted curve in Fig. 4b). The conversion is based on the sdB evolutionary models with sdB masses of 0.35–0.75 $M_\odot$ and envelope masses 0.000–0.006 $M_\odot$ (see Fig. 2d).

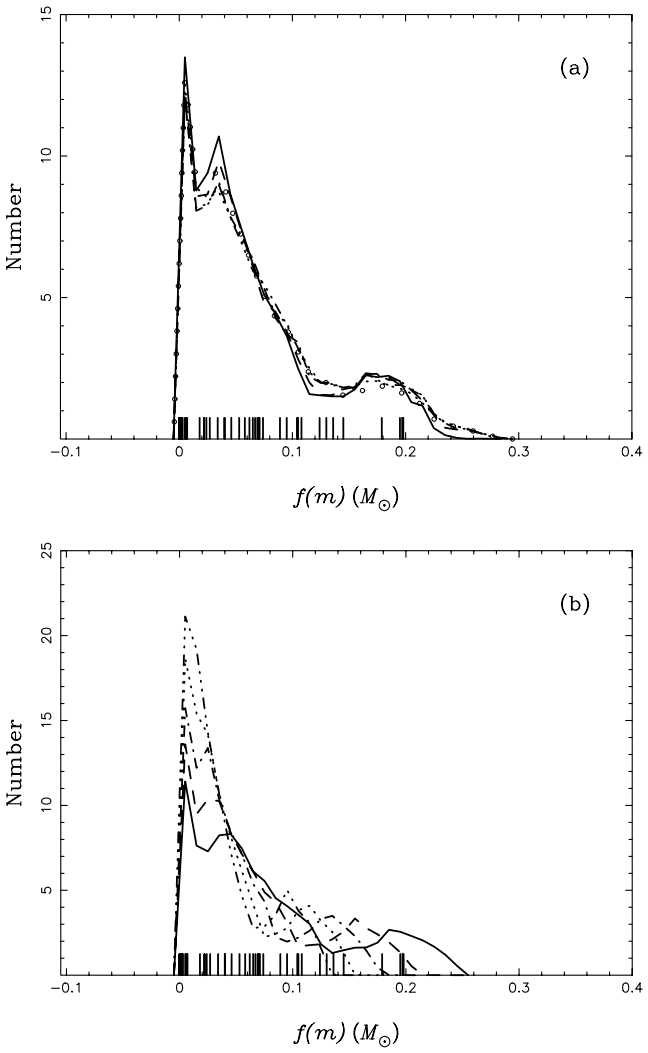

Figure 6. The distribution of the mass function [$f(m) = M_2^3 \sin^3 i/(M_1 + M_2)^2$, M_2 is the mass of the WD, M_1 is the mass of the sdB star]. (a) For the models in Fig. 4(b) (the different models more or less coincide). The inclination is assumed to be uniformly distributed in solid angle. The short ticks along the $f(m)$ axis are based on observed systems (Maxted et al. 2001; Morales-Rueda et al. 2002). The distributions generally show three peaks. The first peak (from the left) is due to the $\sin^3 i$ factor, the second peak corresponds to WD masses between 0.55 and 0.65 $M_\odot$, and the third peak to WD masses between 0.25 and 0.45 $M_\odot$. (b) For the favoured model with $\alpha_{\rm CE} = 0.75$, $\alpha_{\rm th} = 0.75$ and $Z = 0.02$ (shown as a dotted curve in Fig. 4b), for different masses of the sdB stars (solid, dashed, dot-dashed, dotted, triple dot-dashed curves are for $M_{\rm sdB} = 0.4$, 0.5, 0.6, 0.7, 0.8 $M_\odot$, respectively; $M_{\rm sdB} = 0.5\,M_\odot$ provides an overall best fit to the observational data points.)

physically quite reasonable, since it suggests that both the ejection of the common envelope and the conversion of thermal (and ionization) energy are efficient processes, but are not perfect. This is consistent with theoretical CE ejection simulations (Taam & Sandquist 2000; Podsiadlowski 2001) and independent constraints from BPS studies of other post-CE binaries with relatively long orbital periods (e.g. certain symbiotic stars and barium stars; see Han et al. 1995a), which require fairly efficient CE ejection.

In Fig. 5, we present various simulated distributions of the best overall model, i.e. the model with $\alpha_{\rm CE} = \alpha_{\rm th} = 0.75$ and $\eta = 0.25$. Figs 5(a) and (b) are scatter diagrams in the $T_{\rm eff}$–log g and HR diagram, respectively. We assumed that the envelope masses are uniformly distributed between 0.0 and 0.006 $M_\odot$. This leads to the concentration of sdB stars in the upper-right part in Fig. 5(a) or the right part in Fig. 5(b) (see Fig. 2b). The bulk of the observed distribution of sdB stars in Fig. 5(a) overlaps nicely with the simulated distribution. The systems that fall outside the theoretical region are the same as those already discussed in Section 3.2. These may be more massive sdB stars or those with larger hydrogen-rich envelopes and may originate from some of the other sdB channels discussed in subsequent sections. There are no observational data points (Maxted et al. 2001) in the lower-right part of Fig. 5(a) as a result of observational selection effects (this point will be addressed in detail in Paper II).

Fig. 6(a) shows the simulated distribution of the mass function for sdB stars and Fig. 6(b) compares the mass function distribution for different masses of the sdB star. While this comparison should not be taken too literally (since it relies on a very simplified and incomplete BPS model), it confirms that a model with an sdB mass of $\sim$0.5 $M_\odot$ provides an overall good fit to the observed distribution, consistent with earlier findings (e.g. Heber 1986).

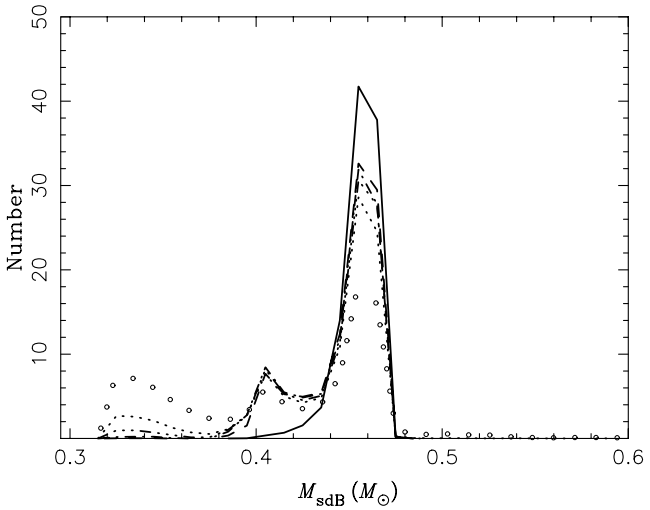

Figure 7. Similar to Fig. 4(b), but for the distribution of masses of sdB stars.

Fig. 7 gives the simulated distributions of masses of sdB stars. The distributions have three peaks – a sharp major peak at 0.46 $M_\odot$, a secondary peak at 0.4 $M_\odot$, and a minor peak at 0.33 $M_\odot$. The major peak is caused by systems with a low-mass ZAMS secondary where the CE is ejected near the tip of the FGB (see Fig. 1). The secondary peak is due to the fact that the range in stellar radius which leads to CE ejection near the tip of the FGB and produces sdB stars is wider for $M_{\rm ZAMS} = 1.90\,M_\odot$ than for $M_{\rm ZAMS} = 1.60\,M_\odot$ (see Table 1). Furthermore CE ejection with $M_{\rm ZAMS} = 1.90\,M_\odot$ results in a low-mass sdB star which has a long helium-core-burning lifetime. The minor peak contains systems that had a ZAMS mass greater than the helium flash mass. The figure shows that almost all the simulated masses of sdB stars are less than 0.48 $M_\odot$, which means that the sparsely scattered dots at $T_{\rm eff} > 35000$ K in Fig. 5 correspond to the post-central-helium-burning phase of sdB stars.

3.4.2 Z = 0.004 simulations

In order to test how the results depend on metallicity, we also performed a series of simulations representing a thick disc population with a metallicity $Z = 0.004$ (Gilmore et al. 1989). These results are shown in Fig. 4(d) (for the same combinations of CE parameters as in Section 3.4.1) and are quite similar to the previous case. However, the middle and the right peaks discussed in Section 3.4.1 merge into a single peak. The reason for this convergence is that lower-metallicity giants are hotter and more compact, and therefore have more tightly bound envelopes. Different WDs then lead to smaller differences between orbital periods for the post-CE systems, causing a merging of the two peaks.

3.5 Discussion

In this section we have shown that helium-burning sdB stars in compact binaries can be formed if the progenitor giants filled their Roche lobe when they were close to the tip of the FGB. Fig. 8 shows the range of orbital periods at the beginning of mass transfer as a function of ZAMS mass for which the core (degenerate if $M_0 \lesssim 1.99\,M_\odot$ for Pop I or $M_0 \lesssim 1.8\,M_\odot$ for $Z = 0.004$) will subsequently ignite helium. Since this is a well-defined evolutionary channel, it provides an excellent diagnostic to test the criterion for the ejection of the CE. In Fig. 9 we plot systems with determined orbital periods in the $T_{\rm eff}$–log g diagram where the size of the symbols indicates the orbital period. There may be a weak hint that the systems with longer orbital periods are less compact and cooler, which implies that they have bigger envelope masses. This would be consistent with simple expectations for CE ejection, since larger remnant envelopes may remain bound to the system if the envelope is ejected at a wider separation. On the other hand, a small fraction of sdB stars may result from CE ejections with $M_0 \gtrsim 1.99\,M_\odot$ for Pop I or $M_0 \gtrsim 1.8\,M_\odot$ for $Z = 0.004$. Since the envelope of these more massive giants are more tightly bound and the orbital energy available in the spiral-in phase is smaller (owing to the smaller orbital period of the pre-CE system), sdB stars produced from more massive giants tend to have very small orbital periods. Most of these sdB stars have fairly low masses ($\sim$0.35 $M_\odot$) and are probably selected against in the observational sample (see Paper II).

Our analysis, however, raises a few further issues. The first is the question whether the orbital parameters that lead to the formation of the compact sdB binary, in particular the orbital period range in

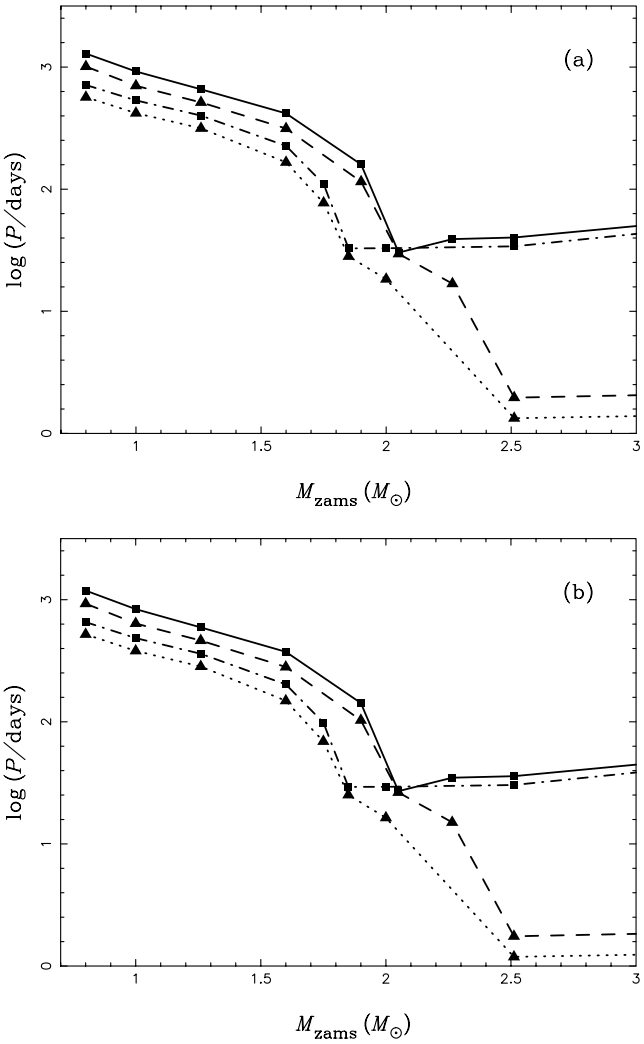

Figure 8. (a) The orbital period range at the beginning of RLOF which leads to a spiral-in phase and the formation of an sdB star in short-period binary for a WD mass of 0.6 $M_\odot$ as a function of ZAMS mass. The dashed and solid curves are for Pop I objects (with overshooting and a 1/4 Reimers' wind). The dotted and the dot-dashed curves are for $Z = 0.004$ (with overshooting and a 1/4 Reimers' wind). (b) Similar to (a), but for a WD mass of 0.3 $M_\odot$.

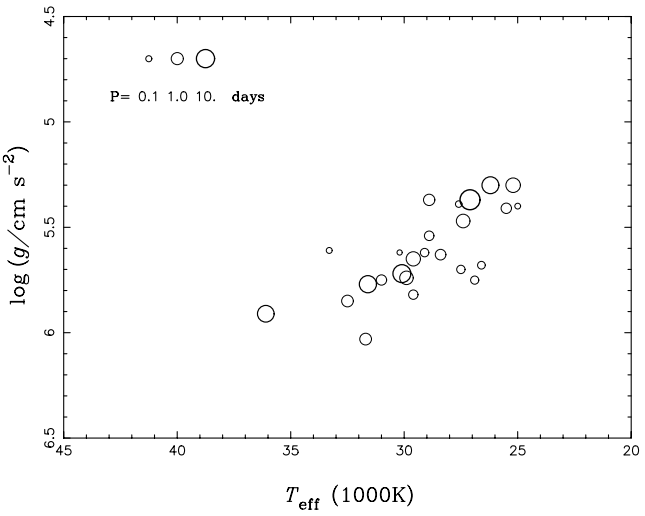

Figure 9. Plot of the distribution of systems with known orbital periods in the $T_{\rm eff}$–log g diagram. Note that sdB stars with long orbital periods appear to have more massive envelopes.

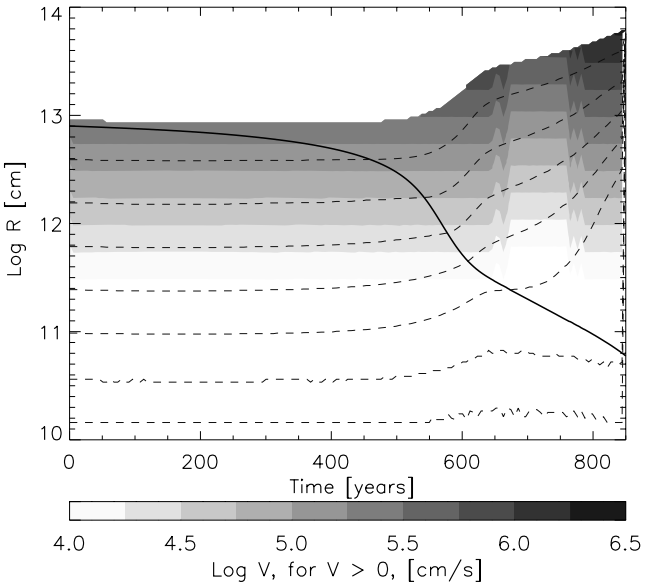

Figure 10. One-dimensional hydrodynamical calculation simulating the spiral-in of a 0.3 $M_\odot$ compact star inside an evolved 1.6 $M_\odot$ giant, illustrating the delayed dynamical instability that occurs when the compact object penetrates into the initially radiative zone below the convective envelope. The thick solid curve indicates the assumed location of the spiralling-in object as a function of time; the dashed curves show the evolution of the radius for various mass coordinates (from bottom to top: 0.4622, 0.4628, 0.4644, 0.4697, 0.4923, 0.6054, 1.113 $M_\odot$). The grey-scale indicates the radial velocity.

Fig. 8, are being realized by actual binaries (note that we do not plot the figure for stars more massive than 3.0 $M_\odot$, as they hardly contribute to the formation of sdB stars because of their tightly bound envelopes). This depends on the previous binary evolutionary phases, which have not been modelled in this paper, but will be addressed in Paper II.

A second problem is that we found that there is no single combination of the CE parameters $\alpha_{\rm CE}$ and $\alpha_{\rm th}$ that produces a perfect fit to the observed period distribution for both metallicities considered. It is quite possible that the observed wide distribution is at least in part a consequence of a large variation of metallicities and possibly even a variation in the CE ejection parameters. Considering how uncertain the theoretical modelling of the CE phase is at present, this would not be very surprising.

Finally we would like to point out an alternative possibility. In recent studies of the dynamics of the CE ejection process, two of the present authors (PhP and NI, see e.g. the discussion in Podsiadlowski 2001) found that, even in cases where the envelope is not ejected in the initial dynamical phase, it will always be ejected at a later stage if the spiralling-in star is relatively compact and penetrates into the initially radiative layer of the giant. An example for such a delayed dynamical ejection is shown in Fig. 10, which represents a one-dimensional, hydrodynamical simulation of the spiral-in of a 0.3 $M_\odot$ compact star spiralling into the envelope of a 1.6 $M_\odot$ giant. The initial spiral-in is very rapid (see the thick solid curve), but slows down once the envelope has expanded significantly and the friction between the spiralling-in binary and the envelope has decreased; in the subsequent slow spiral-in, the envelope is close to hydrostatic equilibrium. However, once the compact object reaches the initially radiative region, a dynamical instability ensues that it is likely to lead to the ejection of the envelope.[2] While this result should only be considered tentative at the moment, we note that the conditions for such a delayed dynamical instability depend mainly on the structure of the giant and cannot be described, even in principle, by a simple α ejection criterion. The characteristic period obtained in this case is of order 0.1 d, similar to the shortest periods of observed sdB binaries. If this is the process that leads to the formation of sdB binaries with the shortest orbital periods, one may expect to see some structure and possibly even some evidence for a bimodal orbital period distribution, for which there is no evidence at the moment.

[2] Our calculations were terminated at this point since they became numerically unstable.

4 THE He WD MERGER CHANNEL

A second channel that can lead to the formation of a single sdB star involves the merger of two He white dwarfs (Webbink 1984; Iben & Tutukov 1986). Close He WD binaries are formed as a result of one or two CE phases (Webbink 1984; Iben & Tutukov 1985; Han et al. 1995a; Iben, Tutukov & Yungelson 1997; Han 1998). If the orbital period is sufficiently short (typically less than 6.76 h for a 0.3 $M_\odot$ + 0.3 $M_\odot$ pair to merge in 15 Gyr), gravitational radiation will cause such a system to shrink until the lighter white dwarf fills its Roche lobe at a typical period of ∼2 min. Mass transfer will be dynamically unstable when the lighter white dwarf is larger than ∼2/3 the mass of the more massive component (Pringle & Webbink 1975; Tutukov & Yungelson 1979; Webbink 1984; Cameron & Iben 1986; Webbink & Iben 1992; Han & Webbink 1999). This leads to its dynamical disruption and the formation of an accretion disc surrounding the more massive white dwarf (Benz et al. 1990). While the subsequent evolution has not been modelled in any detail, it is probably reasonable to expect that a large part of this accretion disc will be accreted by the more massive component. This accretion will initially occur on a dynamical time-scale, but, as the mass in the disc decreases and the disc expands, the accretion rate will decrease and be ultimately determined by the internal viscous processes that govern the evolution of the disc. As the mass of the white dwarf increases, there will be a point at which helium is ignited in a shell and the star will subsequently become a helium-core-burning sdB star owing to the

inward propagation of these nuclear burning shells (Saio & Nomoto 1998; Saio & Jeffery 2000). Unlike the other scenarios considered in this paper, this sdB star will be a single object.

4.1 The conditions for He ignition in He WD mergers

The conditions for helium ignition depend on the initial mass of the more massive white dwarf, its initial thermal structure (i.e. its cooling age) and the accretion history. To determine these, we carried out a series of detailed accretion calculations where we varied the initial mass of the massive white dwarf from 0.2 to 0.4 $M_\odot$ and its initial cooling age. Specifically, we took the initial WD models from the degenerate core of a 1 $M_\odot$ evolutionary calculation and allowed this model to cool for 0.1, 2 and 5 Gyr, respectively. At that point we assumed that they started to accrete pure helium at the maximum rate such that the white dwarf did not expand drastically (we included the compressional heating due to the added mass, but not the potential energy of the accreted matter). This rate was adjusted continuously, so that the radius of the accreting white dwarf never exceeded 0.1 $R_\odot$.

Fig. 11(a) presents an example of such an accretion calculation. It shows the mass accretion rate as a function of the total WD mass for a white dwarf that initially had a mass of 0.2 $M_\odot$ and had cooled for 0.1 Gyr before the onset of accretion. The critical $\dot{M}$ initially increases to reach a maximum value of $\sim 10^{-6}$ $M_\odot$ yr^{-1}, which is determined by the maximum radius adopted for the accreting star. It should be noted that this expansion already occurs at an accretion rate that is substantially smaller than the Eddington-limited accretion rate ($\sim 2 \times 10^{-5}\,M_\odot\,\mathrm{yr}^{-1}$). As the white dwarf continues to accrete, the value of $\dot{M}$ that keeps the white dwarf at this specified radius first decreases and then rises because the more massive white dwarf has a smaller equilibrium radius. Fig. 11(b) is another example, but for an initial He WD mass of 0.25 $M_\odot$.

For each combination of initial WD mass and cooling age, we varied the amount of matter, ΔM, that was accreted and then followed the subsequent evolution until either helium was ignited or the white dwarf had become a cool fully degenerate object. In Table 2 we list the total mass of the model that just ignited helium and the model that did not, respectively, as well as the mass coordinate $M_{\rm ignition}$ at which helium ignition occurs in the former models. The minimum mass for helium ignition varies from $\sim$0.38 $M_\odot$ for the white dwarf with the lowest initial mass to $\sim$0.45 $M_\odot$ for the most massive ones (see Fig. 12). This overall behaviour is determined by the initial thermal structure of the white dwarf and how it changes as a result of the rapid accretion. Since the white dwarf becomes more centrally concentrated as its mass increases, and since the accretion time-scale is much shorter than the characteristic cooling time-scale, compressional heating will make the white dwarf less degenerate. This lowers the critical mass for helium ignition [the minimum mass for helium ignition in non-degenerate stars is 0.3 $M_\odot$ (e.g. Kippenhahn & Weigert 1990)]. Since a white dwarf of lower mass becomes less degenerate during the accretion phase, helium is ignited at a lower critical mass. For each mass, the initially cooler white dwarf can accrete at a higher rate, hence ignite helium at a lower mass. Note that ignition generally occurs off-centre, in most cases at a point larger than the initial mass of the white dwarf (see the last column in Table 2). We are unable to follow the details of the He flash, but assume that the nuclear burning front that starts to propagate towards the centre after helium ignition will ignite the rest of the core [see the simulations by Saio & Nomoto (1998) and Saio & Jeffery (2000)] and that the resulting helium-core-burning star can be modelled as in Section 3.2.

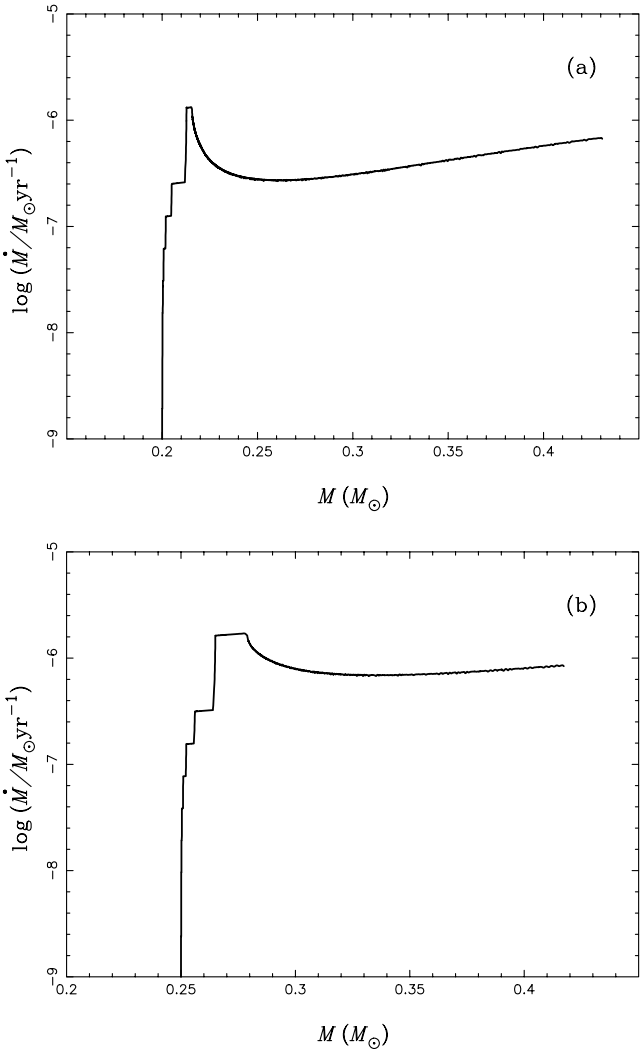

Figure 11. Mass accretion rate as a function of total mass for initial He WD masses of (a) 0.20 $M_\odot$ and (b) 0.25 $M_\odot$ with cooling ages of 0.1 Gyr accreting at the maximum rate that does not cause significant radius expansion.

4.2 Monte Carlo simulation of the merger products

In Fig. 13 we show a simulated distribution of the total mass of the merger product. These were obtained using the BPS code developed by HPE, which is further discussed in Paper II, for a fairly standard set of assumptions. In particular, this simulation assumed a Miller–Scalo initial mass function (Miller & Scalo 1979) for the primary, a flat mass ratio distribution (Mazeh et al. 1992; Goldberg & Mazeh 1994) and a distribution flat in $\log a$, where a is the orbital separation. The star formation rate (SFR) was assumed to be constant with a rate of one binary with a primary more massive than 0.8 $M_\odot$ formed per year during the Galactic lifetime, taken to be 15 Gyr. We again considered a Population I metallicity of $Z = 0.02$ and a typical thick-disc metallicity of $Z = 0.004$ (note, however, that in this case the stellar models did not include a stellar wind or convective overshooting). For each metallicity we considered two combinations for the CE efficiencies; a very efficient model (with $\alpha_{\rm CE} = \alpha_{\rm th} = 1$) and a less efficient model with $\alpha_{\rm CE} = \alpha_{\rm th} = 0.5$ (see Section 3.4). As Fig. 13 shows, the four resulting distributions are confined to a relatively narrow range in mass from $\sim$0.4 to

Table 2. The minimum merger masses for helium ignition.[a]

$M_1^{\rm He}$ ($M_\odot$)	Age (Gyr)	$M_{\rm no-flash}$ ($M_\odot$)	$M_{\rm flash}$ ($M_\odot$)	$M_{\rm ignition}$ ($M_\odot$)
0.20	0.1	0.3860	0.3871	0.0017
0.20	1.0	0.3801	0.3812	0.1860
0.20	5.0	0.3768	0.3778	0.2036
0.25	0.1	0.3947	0.3958	0.2209
0.25	1.0	0.3822	0.3833	0.2485
0.25	5.0	0.3791	0.3800	0.2537
0.30	0.1	0.4040	0.4051	0.2969
0.30	1.0	0.3913	0.3923	0.3001
0.30	5.0	0.3908	0.3915	0.3037
0.35	0.1	0.4234	0.4252	0.3506
0.35	1.0	0.4184	0.4202	0.3541
0.35	5.0	0.4171	0.4186	0.3595
0.40	0.1	0.4541	0.4555	0.4038
0.40	1.0	0.4516	0.4531	0.4100
0.40	5.0	0.4535	0.4544	0.4133

[a] $M_1^{\rm He}$ = initial mass of the more massive He WD; Age = cooling age of the He WD; $M_{\rm no\text{-}flash}$ = maximum total mass after accretion for which no He flash occurs; $M_{\rm flash}$=minimum total mass after accretion for which a He flash occurs; $M_{\rm ignition}$ = ignition point, i.e. the mass coordinate in the white dwarf, at which helium ignites.

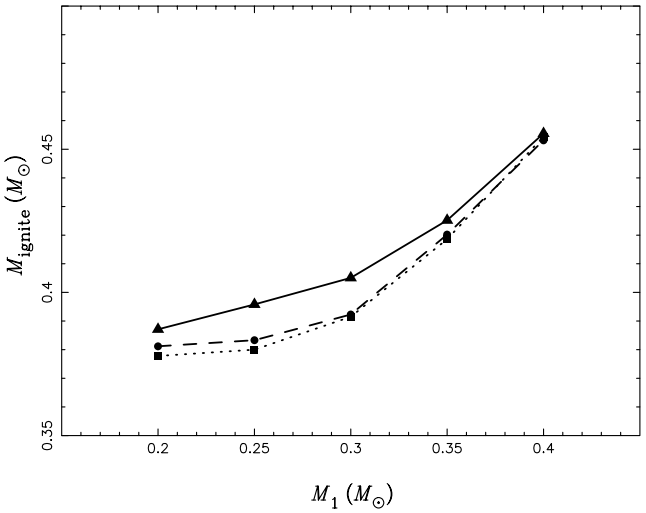

Figure 12. Minimum WD mass at which He is ignited as a function of initial He WD mass, for different cooling ages: solid curve, 0.1 Gyr; dashed curve, 1.0 Gyr; dotted curve, 5 Gyr).

$\sim$0.65 $M_\odot$ (also see Iben & Tutukov 1986). The lower limit is just determined by the minimum mass for helium ignition (see Table 2), while the upper limit is a consequence of the previous binary evolution and the time-scale for merging set by gravitational radiation (see Iben & Tutukov 1986). These distributions appear not to be very sensitive to the assumed metallicity, but seem to depend on the CE ejection parameters: the more efficient the CE ejection, the wider the distribution. The distribution has a peak around 0.52 $M_\odot$. Figs 14(a) and (b) display the $T_{\rm eff}$–log g diagram and HR diagram of the merger products in these simulations.

4.3 Discussion

As Fig. 13 shows, the merger of two He white dwarfs leads to a mass distribution for the resulting sdB stars that is similar to the sdB stars formed from the CE ejection channel, although this channel also allows the formation of more massive objects. The birth rates for sdB stars in these simulations are: 4.6×10^{-3} yr^{-1} (set 1), 6.5×10^{-3} yr^{-1} (set 2), 8.3×10^{-3} yr^{-1} (set 3) and 1.0×10^{-2} yr^{-1} (set 4), respectively. These rates are slightly, but not dramatically, lower than the observationally deduced rates of 2×10^{-14} pc^{-3} yr^{-1} or 0.01 yr^{-1} (by taking an effective Galactic volume of 5×10^{11} pc^3) (Heber 1986). Even though these estimates are quite uncertain (the SFR for $Z = 0.004$ is almost certainly much lower than the SFR for $Z = 0.02$), they still suggest that a significant fraction of sdB stars may form through this channel. This could help to explain some of the sdB stars that appear to be more massive than $\sim$0.5 $M_\odot$ (see Section 3.2), provided that these are single objects.

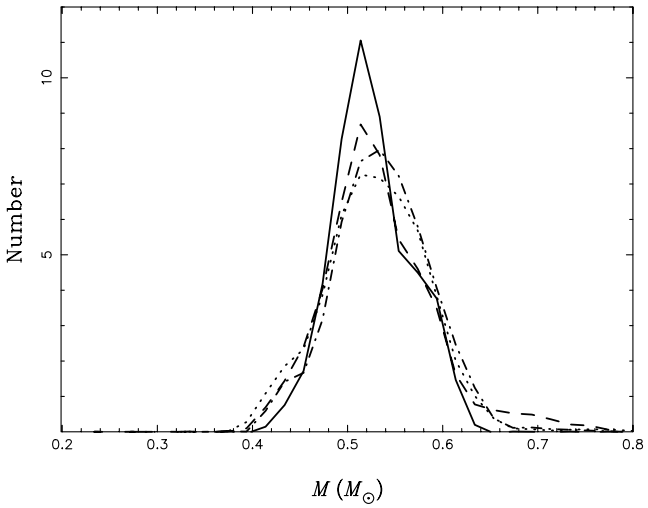

Figure 13. The mass distribution of the He + He WD merger product. Solid, dashed, dot-dashed and dotted curves are for simulation sets 1, 2, 3 and 4, respectively. Simulation set 1 is for $Z = 0.02$, $\alpha_{\rm CE} = 0.5$, $\alpha_{\rm th} = 0.5$; simulation set 2 is for $Z = 0.02$, $\alpha_{\rm CE} = 1.0$, $\alpha_{\rm th} = 1.0$; simulation set 3 is for $Z = 0.004$, $\alpha_{\rm CE} = 0.5$, $\alpha_{\rm th} = 0.5$; simulation set 4 is for $Z = 0.004$, $\alpha_{\rm CE} = 1.0$, $\alpha_{\rm th} = 1.0$.

Note, however, that to obtain the distribution in Fig. 13, we assumed that the mass of the merger product was the sum of the initial masses of the two He white dwarfs. This is clearly an upper limit, since some of the mass of the disrupted lighter white dwarf may remain in a disc around the massive component, possibly forming asteroids and perhaps even planets in due course (Podsiadlowski, Pringle & Rees 1991; Livio, Pringle & Saffer 1992). The detection of any circumstellar material could potentially provide an observational test for sdB stars formed through this channel.

A second uncertainty is related to the amount of hydrogen left in the merged object. Any hydrogen left from the envelopes of either white dwarf component that is mixed with helium and is buried deep inside the merged object immediately after the merger will ignite violently and be quickly consumed, altering the thermal structure of the affected layers in the process (an effect not included in our accretion calculations). We would therefore generally expect that sdB stars from the merger channel have relatively small H-rich envelopes and are therefore hotter and more compact than their counterparts with more massive H-rich envelopes.

5 THE STABLE ROCHE LOBE OVERFLOW CHANNEL

A third channel that can produce an sdB star, and in many respects perhaps the simplest, involves stable mass transfer where a low-mass

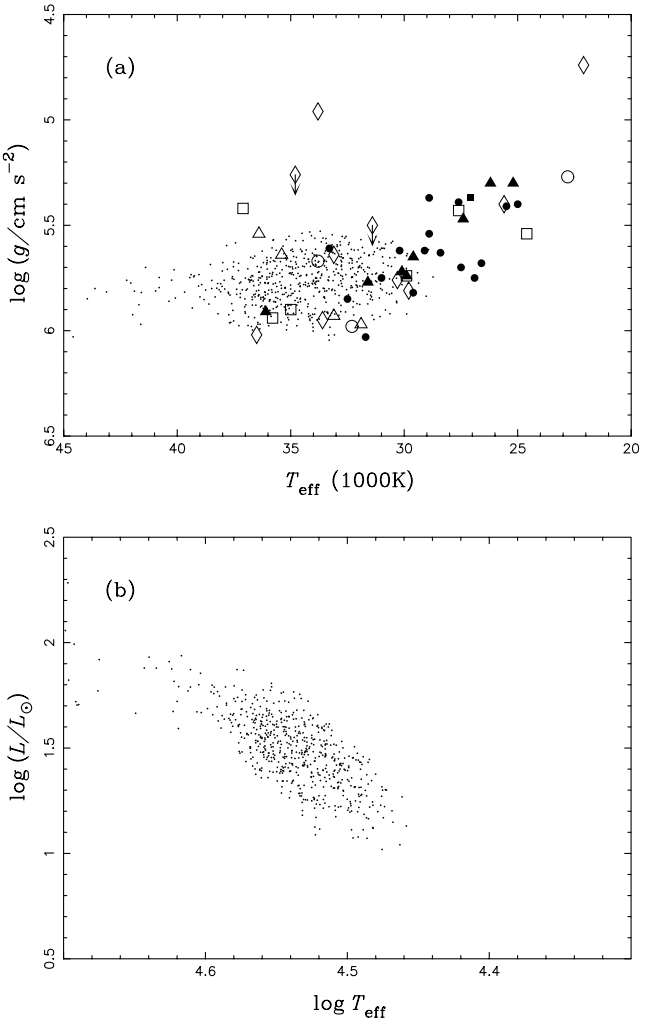

Figure 14. Simulated distribution in the (a) $T_{\rm eff}$–log g and (b) HR diagram for simulation set 1 ($Z = 0.02$, $\alpha_{\rm CE} = 0.5$, $\alpha_{\rm th} = 0.5$). We assume that the masses of the envelopes of He WD mergers are uniformly distributed between 0 and 0.001 $M_\odot$.

giant fills its Roche lobe on the FGB and loses most of its envelope as a result of stable Roche lobe overflow (RLOF). Mass transfer stops once the mass in the H-rich envelope is sufficiently reduced and the radius of the mass-losing component starts to shrink. If the mass of the degenerate core is large enough (see Section 3.1), it will still experience a helium flash and the star may appear as a helium-core-burning sdB star in a binary. Unlike the CE channel, the system will be in a fairly wide binary with orbital periods $\gtrsim$1000 d (instead of $\lesssim$10 d).

This channel has received relatively little attention in the past. This is at least in part due to a widely held theoretical misconception concerning the condition for dynamical mass transfer (see the discussion in Podsiadlowski 2001). As is well known, if a fully convective star (modelled as a polytrope with a polytropic index $n = 1.5$) loses mass, its radius increases, while the Roche lobe radius decreases if the mass donor is more massive than the accreting component. This means that the mass donor will overfill its Roche lobe by an ever-increasing amount, leading to mass transfer on a dynamical time-scale, the formation of a common envelope and a spiral-in phase (as discussed in Section 3). If mass transfer is conservative, the critical mass ratio is $\sim 2/3$, i.e. mass transfer would be dynamically unstable if the mass donor has a mass larger than 2/3 the mass of the companion star. Since the minimum mass for a Population I star that can become a giant is $\sim$0.9 $M_\odot$ in a Hubble time, this would imply that the minimum companion mass has to be larger than $\sim$1.4 $M_\odot$, i.e. similar to the Chandrasekhar mass for a white dwarf. Thus, if it were appropriate to treat a $\sim$1 $M_\odot$ giant as an $n = 1.5$ polytrope, the parameter space for stable RLOF would be exceedingly small.

However, this argument is not correct for a variety of reasons. First, it makes several severe simplifications.(1) Giant stars cannot be modelled as fully convective polytropes, since they have large degenerate cores. This increases the critical mass ratio for dynamical mass transfer substantially (Hjellming & Webbink 1987). (2) The condition for dynamical instability also depends on the amount of mass and angular momentum that is lost from the system (see e.g. Podsiadlowski, Joss & Hsu 1992; Soberman, Phinney & van den Heuvel 1997; Han et al. 2001). (3) Mass loss due to a stellar wind prior to the onset of mass transfer may significantly reduce the mass of the giant (and increase the fractional mass of the degenerate core). This mass loss could be significantly enhanced due to the tidal interaction with the companion (Eggleton & Tout 1989).

A second and perhaps even more fundamental problem with the simplistic application of such a criterion is that it does not take into account the detailed dynamics of the mass transfer process, in particular during the turn-on phase in which a substantial amount of mass is already lost before the dynamical instability occurs. Several recent full binary evolution calculations have shown that the simplistic criterion used in most binary BPS studies to date is not really appropriate. For example, Tauris & Savonije (1999) and Podsiadlowski, Rappaport & Pfahl (2002) have shown in the case of (sub-)giants transferring mass to a neutron star of 1.3/1.4 $M_\odot$ that mass transfer is dynamically stable for all giants up to a mass of $\sim$2 $M_\odot$ [see also Podsiadlowski et al. (1994) for an earlier example involving massive stars]. On the observational side, it has long been clear that quite a few systems that should experience dynamical mass transfer and a CE phase appear to be able to avoid it (see the discussion and references in Podsiadlowski et al. 1992). In the context of sdB stars, Green et al. (2000) have argued strongly that some sdB stars appear to have companions with large separations. This is consistent with the findings of Maxted et al. (2001), since a fraction of the sdB stars in their sample show low radial velocity variations suggesting that they are either single or in fairly wide binaries. A detailed reappraisal of the conditions for dynamical mass transfer is beyond the scope of the present paper and will be published elsewhere (Podsiadlowski & Han, in preparation). Here we restrict ourselves to examining the conditions under which stable mass transfer leads to the formation of an sdB star in a wide binary.

5.1 The conditions for stable RLOF and the formation of sdB stars in wide binaries

To determine the conditions for the formation of sdB stars through the stable RLOF channel, we performed a series of binary stellar evolution calculations for mass donors with different masses on the ZAMS, ranging from 0.8 to 1.9 $M_\odot$. For each mass, we systematically varied the mass of the core at the beginning of mass transfer and the mass of the companion star. In these calculations we assumed that mass transfer was completely non-conservative, and that all the mass that was lost from the system carried with it the orbital angular momentum of the accreting component (as appears to be most appropriate if the accretor is a white dwarf). In the standard set of calculations, we included a Reimers-type wind with $\eta = 1/4$ (see

Table 3. Critical masses for stable RLOF.[a]

$M_1^{\rm ZAMS}$ ($M_\odot$)	$M_{\rm c}$ ($M_\odot$)	$M_1^{\rm RLOF}$ ($M_\odot$)	$M_2^{\rm min}$ ($M_\odot$)	$q_{\rm crit}$
0.80	0.1992	0.7974	0.6243	1.2773
0.80	0.2494	0.7945	0.6071	1.3087
0.80	0.2996	0.7866	0.6071	1.2957
0.80	0.3501	0.7683	0.6090	1.2616
0.80	0.3994	0.7328	0.5888	1.2446
0.80	0.4486	0.6696	0.5225	1.2815
1.00	0.1994	0.9975	0.8049	1.2393
1.00	0.2498	0.9953	0.7898	1.2602
1.00	0.2992	0.9894	0.7968	1.2417
1.00	0.3493	0.9759	0.8229	1.1859
1.00	0.3995	0.9496	0.8354	1.1367
1.00	0.4482	0.9055	0.8185	1.1063
1.26	0.1994	1.2577	1.0339	1.2165
1.26	0.2493	1.2560	1.0283	1.2214
1.26	0.2993	1.2515	1.0452	1.1974
1.26	0.3494	1.2414	1.0804	1.1490
1.26	0.3985	1.2227	1.1149	1.0967
1.26	0.4483	1.1905	1.1134	1.0692
1.60	0.2483	1.5968	1.3402	1.1915
1.60	0.2991	1.5941	1.3366	1.1927
1.60	0.3486	1.5873	1.3943	1.1384
1.60	0.3981	1.5741	1.4494	1.0860
1.60	0.4472	1.5522	1.4696	1.0562
1.90	0.2495	1.8969	1.5477	1.2256
1.90	0.2963	1.8959	1.6066	1.1801
1.90	0.3488	1.8920	1.6366	1.1561
1.90	0.3982	1.8827	1.7322	1.0869

[a] $M_1^{\rm ZAMS}$ = ZAMS mass of the primary; $M_{\rm c}$ = the core mass of the primary at the onset of RLOF; $M_1^{\rm RLOF}$ = the surface mass of the primary at the onset of RLOF; $M_2^{\rm min}$ = minimum mass of the companion (WD/NS) for stable RLOF; $q_{\rm crit}$ = the critical mass ratio.

equation 2) before the mass transfer phase. We switched this wind off once the mass transfer rate exceeded the value given by equation (2) by a factor of 100 and did not include stellar wind mass loss after the end of the mass transfer phase. In each calculation, we first checked whether mass transfer was dynamically stable. In cases where mass transfer is dynamically unstable, there is no solution for the mass transfer rate, $\dot{M}$, for which the radius of the secondary can be equal to the Roche lobe radius [see Han et al. (2000) for the treatment of the surface boundary condition]. If mass transfer is stable, we continued mass transfer until the mass donor started to shrink below its Roche lobe, terminating the mass transfer phase. If, at this point, the mass of the H-exhausted core exceeded the appropriate minimum core mass for subsequent helium ignition[3] (as determined in Section 3.1[4]), it may appear as a helium-core-burning sdB star.

The results of these calculations are summarized in Tables 3 and 4, which show for each ZAMS mass the core mass and the total mass of the mass donor at the beginning of mass transfer and the minimum mass of the secondary (and critical mass ratio) for which mass transfer is stable and leads to the formation of a helium-burning sdB star. These results demonstrate, as discussed above, that mass transfer is dynamically stable even if the mass donor is substantially more massive than the secondary and that sdB stars can form through this channel without any non-standard assumptions. For stars with ZAMS masses $\geqslant 1.6\ M_\odot$, the secondary mass has to be larger than $1.34\ M_\odot$, which is similar to the maximum mass of a white dwarf, and hence does not correspond to realistic systems with white dwarf accretors. Note that, for each mass, the critical mass ratio tends to decrease for the initially more evolved systems, since for these the evolutionary time-scale is shorter and hence the mass transfer rate higher than for the less-evolved ones. This has the consequence that the core mass grows less during the mass transfer phase. One may also notice that some of the behaviour in Table 3 is non-monotonic. The non-monotonic behaviour of $q_{\rm crit}$ at the lowest $M_{\rm c}$ is caused by primaries with a core mass $M_{\rm c}$ near the base of the FGB, where the core is not very degenerate and the envelope is not yet fully convective. The non-monotonic behaviour for $0.8\ M_\odot$ stars with the largest $M_{\rm c}$ is a consequence of its thin envelope mass.

While these calculations show that sdB stars can form in wide binaries without any non-standard assumptions, it is quite plausible, perhaps even likely, that the wind mass-loss rate before the beginning of the RLOF phase will be enhanced due to the tidal interaction with the companion (as originally proposed by Eggleton & Tout 1989). The main effect that this has is to increase the overall parameter space for which this channel produces sdB stars in wide binaries. This is illustrated in Fig. 15, which shows the minimum mass of the accreting white dwarf as a function of the ZAMS mass of the donor for the standard model used above and two sequences of calculations, where we assumed that the pre-RLOF wind mass-loss rate was enhanced by a factor of 4 and 8, respectively (i.e. we took $\eta = 1$ and 2).

5.2 Binary calculations

Fig. 16 shows a representative binary calculation from one of the sequences in the previous section for a star with a ZAMS mass of $1\ M_\odot$. At the beginning of mass transfer, the mass donor has a core mass of $0.3975\ M_\odot$ and a total mass of $0.9508\ M_\odot$, and the mass of the companion star is $0.84\ M_\odot$. With these parameters, mass transfer starts at an orbital period of 348.4 d. Initially, mass transfer occurs on a thermal time-scale and reaches a maximum of $\sim 4 \times 10^{-4}\ M_\odot\ {\rm yr}^{-1}$. After the mass ratio has been reversed and the star has regained thermal equilibrium, mass transfer settles to a rate of $\sim 4 \times 10^{-7}\ M_\odot\ {\rm yr}^{-1}$ and gradually decreases as the secondary ascends the giant branch. Once the mass in the H-rich envelope drops below $0.021\ M_\odot$, the secondary shrinks below the Roche lobe and mass transfer stops. As the remnant envelope collapses, the secondary quickly moves across the HR diagram and ultimately becomes an sdB star of $0.4745\ M_\odot$ in a wide binary with an orbital period of 948.9 d.

Whether the secondary becomes an sdB star and its location in both the $T_{\rm eff}$–$\log g$ and the HR diagram also depend on mass loss via a stellar wind after the RLOF phase. For example, consider a binary with an orbital period of 606 d consisting of a giant with a total mass of $0.9206\ M_\odot$ and a core mass of $0.4343\ M_\odot$ (which corresponds to one of the sequences with a $1\ M_\odot$ ZAMS star) in orbit with a $0.82\ M_\odot$ white dwarf. If wind mass loss is switched off once the system has entered the RLOF phase, the giant starts to ignite helium when its core mass reaches $0.4731\ M_\odot$, but its total mass is still $0.5210\ M_\odot$ (the system has an orbital period of 1306 d at this point). If there is no further mass loss, the secondary

[3] In Table 4, the WD mass adopted is small as possible, or as close as possible to a typical WD mass of $0.6\ M_\odot$. Note, however, that, for a higher WD mass, RLOF is more stable and the mass transfer rate is lower. As a consequence, the core can grow more massive, making He ignition more likely. In this case, the minimum orbital period P for the formation of an sdB star could be lower than indicated in the table.

[4] In a number of cases, we continued the calculations up to the point of helium ignition to confirm that the limits determined in Section 3.1 are also applicable in this case.

Table 4. Minimum core mass and orbital period for stable RLOF to form an sdB star.[a]

$M_1^{\rm ZAMS}$ ($M_\odot$)	$M_1^{\rm RLOF}$ ($M_\odot$)	M_2 ($M_\odot$)	$M_{\rm c}$ ($M_\odot$)	$\log(P/{\rm d})$	$q_{\rm RLOF}$	$\log(P_{\rm sdB}/{\rm d})$	$M_{\rm sdB}$ ($M_\odot$)	$q_{\rm sdB}$
0.80	0.7376	0.7263	0.3940	2.6218	1.0537	2.9118	0.4570	0.6526
1.00	0.9632	0.9023	0.3771	2.3986	1.0822	2.9097	0.4552	0.5112
1.26	1.2387	1.1310	0.3587	2.1596	1.0962	2.9097	0.4550	0.4022
1.60	1.5902	1.4556	0.3319	1.7989	1.0967	2.8460	0.4425	0.3049
1.90	1.8964	1.7234	0.2793	1.2613	1.1006	2.6022	0.4064	0.2354

[a] $M_1^{\rm ZAMS}$ = ZAMS mass of the primary; $M_1^{\rm RLOF}$ = the surface mass of the primary at the onset of RLOF; M_2 = the mass of the companion (WD/NS) adopted (close to the minimum mass for stable RLOF according to the results in Table 3); $M_{\rm c}$ = the core mass of the primary at the onset of RLOF (RLOF before the core mass reaches $M_{\rm c}$ will not result in a helium-burning sdB); P = the orbital period (in days) at the onset of RLOF; $q_{\rm RLOF}$ = the mass ratio at the onset of RLOF; $P_{\rm sdB}$ = the orbital period of the sdB star formed; $M_{\rm sdB}$ = the mass of the sdB star formed; $q_{\rm sdB}$ = the mass ratio of the sdB binary.

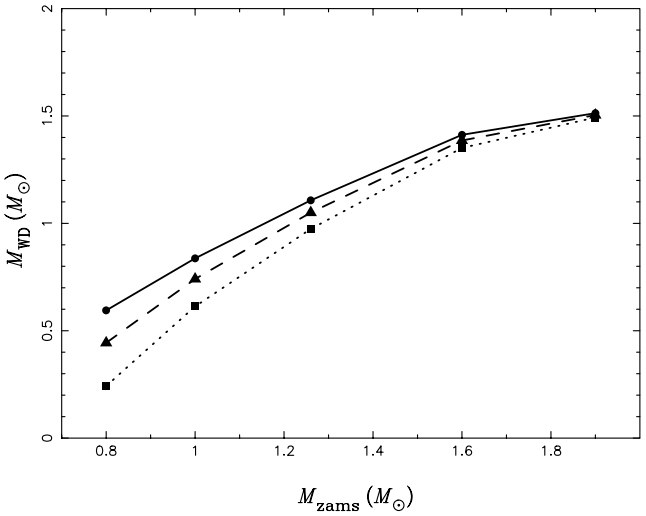

Figure 15. Minimum WD mass for stable RLOF (see Tables 3 and 4) as a function of ZAMS mass that leads to the formation of an sdB star. The solid curve is for a one-quarter Reimers' wind, dashed and dotted curves are for Reimers' wind mass-loss rate with $\eta = 1$ and $\eta = 2$ (i.e. significantly enhanced wind loss rate; e.g. due to tidal interactions).

will then settle on the normal horizontal branch, burn helium in the core and then ascend the AGB [this typically requires an envelope mass larger than $\sim$0.05 $M_\odot$ (see Dorman, Rood & O'Connel 1993)]. On the other hand, if wind mass loss is not switched off during the RLOF phase but continues at a rate of one-quarter of the Reimers rate, the total mass is 0.4864 $M_\odot$ when helium is ignited in the core of mass 0.4731 $M_\odot$. In this case it has the appearance of an sdB star lying in the upper-right corner of the $T_{\rm eff}$–log g diagram.

5.3 Discussion

As we have shown in this section, stable RLOF provides a third channel for the formation of sdB stars. These will generally be in wide binaries with typical orbital periods of 400–1500 d. The mass distribution is similar to the distribution in the CE channel. However, one might expect that the envelope masses could be systematically larger than in the CE ejection case, since the orbital period is much longer, which means that a larger envelope mass may remain bound to the degenerate core when the donor becomes detached. This would suggest that sdB stars formed through this channel would be less compact and cooler than their counterparts from the CE channel.

The importance of this channel is difficult to assess. While standard assumptions lead to the formation of sdB stars, the allowed range for the binary parameters is probably quite small in this model, since it requires relatively massive white dwarfs, which are not very common. However, this parameter range could be dramatically increased if the stellar wind mass-loss rate is significantly enhanced, e.g. due to the tidal interaction with the companion star (Tout & Eggleton 1988). On the other hand, observational surveys could in principle allow the calibration of such enhanced stellar winds.

One may notice that we only deal with WD companions in this section, though stable RLOF with MS companions can also produce sdB stars. Observational surveys show that at least half of all sdB stars have cool MS companions (see Section 1). This seems to be in contradiction with the observations by Maxted et al. (2001) that the majority of sdB stars are short-period binaries with WD companions, as it implies a binary fraction larger than unity. The contradiction is due to various observational selection effects, and will be addressed in Paper II.

In this section, we made the simplifying assumption that mass transfer to a WD companion is completely non-conservative in the stable RLOF channel. This assumption is appropriate for low mass transfer rates, where nova explosions are believed to be effective in expelling all of the transferred matter, but probably not for higher rates (larger than $\sim 10^{-7}\,M_\odot\ {\rm yr}^{-1}$), where the white dwarf may be able to accrete most of the transferred matter and burn it steadily (as in supersoft X-ray binaries). On the other hand, for even higher rates the white dwarf will start to swell up (Nomoto, Nariai & Sugimoto 1979) and may then lose most of the transferred mass again, possibly in the form of an optically thick wind (Hachisu, Kato & Nomoto 1996). Clearly all of these effects need to be studied further and should be included in future studies.

6 SUMMARY

In this paper, we have demonstrated that the three binary evolution channels that have been proposed for the formation of sdB (and related sdO/sdOB) stars may all contribute to the observed population.

In the CE ejection channel, which may account for more than two-thirds of all sdB stars, dynamically unstable mass transfer near the tip of the FGB results in the formation of a CE and spiral-in phase, leaving a short-period binary after the envelope has been ejected. The system becomes an sdB binary if helium is ignited. Using detailed stellar evolution calculations, we have determined how close to the tip of the FGB the progenitor has to be at the onset of RLOF. Using simplified binary population synthesis calculations,

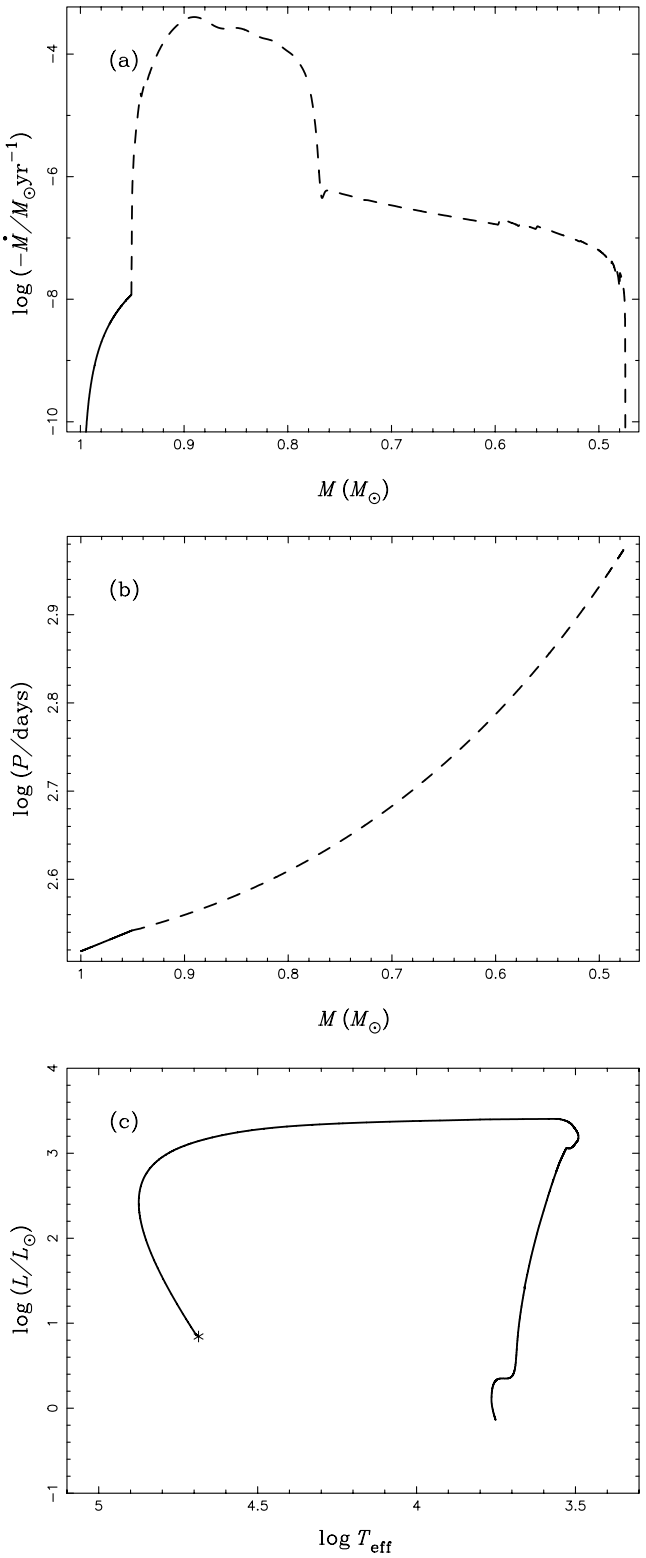

Figure 16. (a) Evolution of mass transfer rate, (b) orbital period as a function of mass, and (c) evolutionary track in the HR diagram, to demonstrate the case of stable RLOF for a binary with a giant donor with an initial mass of 1 $M_\odot$ and a 0.84 $M_\odot$ WD companion (Pop I, with overshooting, one-quarter Reimers' wind). The solid curves in (a) and (b) show the evolution before the onset of RLOF, i.e. due to a stellar wind. No stellar wind was included during and after RLOF.

we have been able to show that the CE ejection process has to be very efficient and that the ionization energy in the envelope has to be included in the ejection criterion in order to be able to explain the observed orbital period distribution.

In the stable RLOF channel, the progenitor system experiences stable mass transfer in which the giant is stripped off its envelope as a result of the mass transfer. If this occurs near the tip of the FGB, the remnant helium core will still ignite helium in the core and become an sdB star in a binary with a long orbital period and a fairly thick hydrogen-rich envelope as compared to the other channels. Using detailed binary evolution calculations, we demonstrated that this channel usually requires a fairly massive white dwarf companion or enhanced stellar wind mass loss before the onset of RLOF (e.g. tidally enhanced winds).

Double He WDs may coalesce due to gravitational wave radiation. When helium is ignited in the merger, a single sdB star is formed, and its hydrogen envelope is likely to be very thin. We have determined the conditions for which the merged system will be able to ignite helium.

In a follow-up paper we will implement these results in full binary population synthesis calculations to assess their relative importance and to allow direct comparison with observed subdwarf populations.

ACKNOWLEDGMENTS

We thank Drs A. Lynas-Gray and S. Yi for many stimulating discussions. We are grateful to Dr O. Pols, the referee, for his valuable suggestions which helped to improve the paper. ZH thanks the Department of Astrophysics, Oxford, for its hospitality. This work was in part supported by a Royal Society UK–China Joint Project Grant (PhP and ZH), the Chinese National Science Foundation under Grants Nos 19925312 and 10073009, and NKBRSF No. 19990754 (ZH).

REFERENCES

Alexander D. R., Ferguson J. W., 1994a, in Jorgensen U. G., ed., Molecules in the Stellar Environment. Springer-Verlag, Berlin, p. 149
Alexander D. R., Ferguson J. W., 1994b, ApJ, 437, 879
Allard F., Wesemael F., Fontaine G., Bergeron P., Lamontagne R., 1994, AJ, 107, 1565
Andersen J., 1991, A&AR, 3, 91
Aznar Cuadrado R., Jeffery C. S., 2001, A&A, 368, 994
Benz W., Cameron A. G. W., Press W. H., Bowers R. L., 1990, ApJ, 348, 647
Bessell M. S., Brett J. M., Scholz M., Wood P. R., 1989, A&AS, 77, 1
Brassard P., Fontaine G., Billères M., Charpinet S., Liebert J., Saffer R.A., 2001, ApJ, 563, 1013
Brown T. M., Ferguson H. C., Davidsen A. F., Dorman B., 1997, ApJ, 482, 685
Cameron A. G. W., Iben I., Jr, 1986, ApJ, 305, 228
Carraro G., Girardi L., Bressan A., Chiosi C., 1996, A&A, 305, 849
Castellani M., Castellani V., 1993, ApJ, 407, 649
Castellani V., Chieffi A., Pulone L., Tornambe A., 1985, ApJ, 296, 204
Caughlan G. R., Fowler W. A., 1988, At. Data Nucl. Data Tables, 40, 284
Caughlan G. R., Fowler W. A., Harris M. J., Zimmerman B. A., 1985, At. Data Nucl. Data Tables, 35, 198
D'Cruz N. L., Dorman B., Rood R. T., O'Connell R. W., 1996, ApJ, 466, 359
Dewi J., Tauris T., 2000, A&A, 360, 1043
Dorman B., Rood R. T., O'Connell R. W., 1993, ApJ, 419, 596
Downes R. A., 1986, ApJS, 61, 569

Eggen O. J., 1985, AJ, 90, 333
Eggleton P. P., 1971, MNRAS, 151, 351
Eggleton P. P., 1972, MNRAS, 156, 361
Eggleton P. P., 1973, MNRAS, 163, 179
Eggleton P. P., Tout C. A., 1989, in Batten A. H., ed., Algols. Kluwer, Dordrecht, p. 164
Ferguson D. H., Green R. F., Liebert J., 1984, ApJ, 287, 320
Fitzpatrick E. L., Garmany C. D., 1990, ApJ, 363, 119
Giannuzzi M. A., 1981, A&A, 103, 111
Gilmore G., Wyse R. F. G., Kuijken K., 1989, ARA&A, 27, 555
Goldberg D., Mazeh T., 1994, A&A, 282, 801
Green E. M., Liebert J., Saffer R. A., 2000, astro-ph/0012246
Green R. F., Schmidt M., Liebert J., 1986, ApJS, 61, 305
Hachisu I., Kato M., Nomoto K., 1996, ApJ, 470, L97
Han Z., 1995, PhD thesis, Cambridge Univ.
Han Z., 1998, MNRAS, 296, 1019
Han Z., Webbink R. F., 1999, A&A, 349, L17
Han Z., Podsiadlowski Ph., Eggleton P. P., 1994, MNRAS, 270, 121 (HPE)
Han Z., Podsiadlowski Ph., Eggleton P. P., 1995a, MNRAS, 272, 800
Han Z., Eggleton P. P., Podsiadlowski Ph., Tout C. A., 1995b, MNRAS, 277, 1443
Han Z., Tout C. A., Eggleton P. P., 2000, MNRAS, 319, 215
Han Z., Eggleton P. P., Podsiadlowski Ph., Tout C. A., Webbink R. F., 2001, in Podsiadlowski Ph., Rappaport S., King A. R., D'Antona F., Burderi L., eds, ASP Conf. Ser., Vol. 229, Evolution of Binary and Multiple Star Systems. Astron. Soc. Pac., San Francisco, p. 205
Heber U., 1986, A&A, 155, 33
Heber U., Moehler S., Napiwotzki R., Thejll P., Green E. M., 2002, A&A, 383, 938
Hjellming M. S., Webbink R. F., 1987, ApJ, 318, 794
Humphreys R. M., Davidson K., 1979, ApJ, 232, 409
Iben I., Jr, Livio M., 1993, PASP, 105, 1373
Iben I., Jr, Renzini A., 1983, ARA&A, 21, 271
Iben I., Jr, Tutukov A. V., 1985, ApJS, 58, 661
Iben I., Jr, Tutukov A. V., 1986, ApJ, 311, 753
Iben I., Jr, Tutukov A. V., Yungelson L. R., 1997, ApJ, 475, 291
Itoh N., Adachi T., Nakagawa M., Kohyama Y., Munakata H., 1989, ApJ, 339, 354 (erratum 1990, ApJ, 360, 741)
Itoh N., Mutoh H., Hikita A., Kohyama Y., 1992, ApJ, 395, 622 (erratum 1993, ApJ, 404, 418)
Jeffery C. S., Pollacco D. L., 1998, MNRAS, 298, 179
Kilkenny D., Koen C., Jeffery J., Hill C. S., O'Donoghue D., 1999, MNRAS, 310, 1119
Kippenhahn R., Weigert A., 1990, Stellar Structure and Evolution. Springer-Verlag, Berlin
Koen C., Orosz J. A., Wade R. A., 1998, MNRAS, 300, 695
Lamers H. J. G. L. M., Fitzpatrick E. L., 1988, ApJ, 324, 279
Livio M., Pringle J. E., Saffer R. A., 1992, MNRAS, 257, L15
Maxted P. F. L., Moran C. K. J., Marsh T. R., Gatti A. A., 2000a, MNRAS, 311, 877
Maxted P. R. L., Marsh T. R., North R. C., 2000b, MNRAS, 317, L41
Maxted P. F. L., Heber U., Marsh T. R., North R. C., 2001, MNRAS, 326, 1391
Mazeh T., Goldberg D., Duquennoy A., Mayor M., 1992, ApJ, 401, 265
Mengel J. G., Norris J., Gross P. G., 1976, ApJ, 204, 488
Miller G. E., Scalo J. M., 1979, ApJS, 41, 513
Morales-Rueda L., Maxted P. F. L., Marsh T. R., Heber U., 2002, MNRAS, submitted
Moran C., Maxted P., Marsh T. R., Saffer R. A., Livio M., 1999, MNRAS, 304, 535
Nomoto K., Nariai K., Sugimoto D., 1979, PASJ, 31, 287
Orosz J. A., Wade R. A., 1999, MNRAS, 310, 773
Paczyński B., 1976, in Eggleton P. P., Mitton S., Whelan J., eds, Structure and Evolution of Close Binaries. Kluwer, Dordrecht, p. 75
Podsiadlowski Ph., 2001, in Podsiadlowski Ph., Rappaport S., King A. R., D'Antona F., Burderi L., eds, ASP Conf. Ser. Vol. 229, Evolution of Binary and Multiple Star Systems. Astron. Soc. Pac., San Francisco, p. 239
Podsiadlowski Ph., Pringle J. E., Rees M. J., 1991, Nat, 352, 783
Podsiadlowski Ph., Joss P. C., Hsu J. J. L., 1992, ApJ, 391, 246
Podsiadlowski Ph., Hsu J. J. L., Joss P. C., Ross R. R., 1994, in Clegg R. E. S., Stevens I. R., Meikle W. P. S., eds, Circumstellar Media in the Late Stages of Stellar Evolution. Cambridge Univ. Press, Cambridge, p. 187
Podsiadlowski Ph., Rappaport S., Pfahl E., 2002, ApJ, 565, 1107
Pols O. R., Tout C. A., Eggleton P. P., Han Z., 1995, MNRAS, 274, 964
Pols O. R., Tout C. A., Schröder K.-P., Eggleton P. P., Manners J., 1997, MNRAS, 289, 869
Pols O. R., Schröder K.-P., Hurley J. R., Tout C. A., Eggleton P. P., 1998, MNRAS, 298, 525
Pringle J. E., Webbink R. F., 1975, MNRAS, 172, 493
Reimers D., 1975, Mem. R. Soc. Liége, 6e Ser., 8, 369
Renzini A., 1981, in Chiosi C., Stalio R., eds, Effects of Mass Loss on Stellar Evolution. Reidel, Dordrecht, p. 319
Rogers F. G., Iglesias C. A., 1992, ApJS, 79, 507
Saffer R. A., Bergeron P., Koester D., Liebert J., 1994, ApJ, 432, 351
Saffer R. A., Livio M., Yungelson L. R., 1998, ApJ, 502, 394
Saio H., Jeffery C. S., 2000, MNRAS, 313, 671
Saio H., Nomoto K., 1998, ApJ, 500, 388
Sargent W. L. W., Searle L., 1968, ApJ, 152, 443
Schröder K.-P., Pols O. R., Eggleton P. P., 1997, MNRAS, 285, 696
Shore S. N., 1988, in ESA, A Decade of UV Astronomy with the IUE Satellite, Vol. 1, p. 67
Soberman G. E., Phinney E. S., van den Heuvel E. P. J., 1997, A&A, 327, 620
Sweigart A. V., 1997, ApJ, 474, L23
Taam R. E., Sandquist E. L., 2000, ARA&A, 38, 113
Tauris T. M., Savonije G. J., 1999, A&A, 350, 928
Thejll P., Ulla A., MacDonald J., 1995, A&A, 303, 773
Tout C. A., Eggleton P. P., 1988, ApJ, 334, 357
Tutukov A. V., Yungelson L. R., 1979, Acta Astron., 29, 665
Ulla A., Thejll P., 1998, A&AS, 132, 1
Ulmer A., Fitzpatrick E. L., 1998, ApJ, 504, 200
Vauclair G., Liebert J., 1987, in Kondo Y., ed., Exploring the Universe with the IUE Satellite, Vol. 1. Reidel, Dordrecht, p. 355
Webbink R. F., 1984, ApJ, 277, 355
Webbink R. F., 1988, in Mikolajewska J., Friedjung M., Kenyon S. J., Viotti R., eds, The Symbiotic Phenomenon. Kluwer, Dordrecht, p. 311
Webbink R. F., Iben I., Jr, 1992, in Davis Philip A. G., Hayes D. S., Liebert J. W., eds, IAU Colloq. No. 95, The Second Conference on Faint Blue Stars. L. Davis Press, Yale, p. 445
Wood J. H., Saffer R., 1999, MNRAS, 305, 820
Yi S., Demarque P., Oemler A., Jr, 1997, ApJ, 486, 201
Yi S., Lee Y., Woo J., Park J., Demarque P., Oemler A., Jr, 1999, ApJ, 513, 128

This paper has been typeset from a TEX/LATEX file prepared by the author.